3 Dynamical Mean-Field Theory for Materials

Eva Pavarini
Peter Grünberg Institute
Forschungszentrum Jülich

Contents

E. Pavarini, E. Koch, A. Lichtenstein, and D. Vollhardt (eds.)
Understanding Correlated Materials with DMFT
Modeling and Simulation Vol. 15
Forschungszentrum Jülich, 2025, ISBN 978-3-95806-813-1
http://www.cond-mat.de/events/correl25

1 Introduction

In 1965, when the two founding papers [1] of density-functional theory (DFT) had just been published in the Physical Review, very few could recognize the revolution in the making. Efficient techniques for materials science applications were missing and computers were not that powerful. And yet in 50 years, thanks to remarkable ideas, novel algorithms and steady advance in computational power, brilliant minds brought DFT to its present splendor, making it the *standard model* of condensed matter physics. In 1998, in his Nobel lecture [2], Walter Kohn, described the most important contributions of DFT to science with these words

> *The first is in the area of fundamental understanding. Theoretical chemists and physicists, following the path of the Schrödinger equation, have become accustomed to think in a truncated Hilbert space of single particle orbitals. The spectacular advances achieved in this way attest to the fruitfulness of this perspective. However, when very high accuracy is required, so many Slater determinants are required (in some calculations up to* $\sim 10^9$*!) that comprehension becomes difficult.*

DFT changed the focus from the N-electron ground-state wavefunction $\Psi(\boldsymbol{r}_1, \ldots, \boldsymbol{r}_N)$ to a three-dimensional variable, the electronic ground-state density $n(\boldsymbol{r})$, or other directly measurable quantities, such as response functions. These, within a given approximation of the DFT exchange-correlation functional, could be calculated *from first principles*, i.e., using as input the type of atoms involved and, at most, their positions. In practice, $n(\boldsymbol{r})$ is obtained by mapping the actual many-body problem onto an auxiliary single-electron Hamiltonian with the same ground-state electron density, the Kohn-Sham Hamiltonian. The associated Kohn-Sham eigenvalues are thus in principle merely Lagrange multipliers. Remarkably, however, the big success of DFT came, in part, from bold applications of the theory beyond its actual realm of validity. To general surprise, the Kohn-Sham eigenvalues turned out to be in many cases excellent approximations to the actual elementary excitations of a given material. Early on it became clear, however, that this Ansatz fails qualitatively for a whole category of systems, those in which local Coulomb repulsion effects are large, also known as *strongly-correlated materials*. Paradoxically, in describing strong-correlation phenomena, simple models describing generic features of the microscopic mechanism are much more effective than DFT-based materials-specific calculations. This happens, e.g., for the Kondo effect, heavy-fermion behavior, or the metal-insulator transition. Thus criticisms arose. Particularly outspoken in this contest was another Nobel laureate, P.W. Anderson, who emphasized the emergent nature of a true many-body phenomenon [3]. Emergent states typically elude a simple mapping to an effective non-interacting system. For a while, two apparently incompatible philosophies thus coexisted. The first-principles school identified in the materials dependence the essential ingredient for understanding the real world, and tried to correct the failures of the practical implementations of DFT by corrections, often ad hoc, of the exchange-correlation potential. Instead, the many-body models school identified canonical models which explain specific emergent phenomena, dismissing the materials dependence as non-relevant, non-generic detail. In the last three decades these different world-views started to merge, and it became apparent that both sides were right and wrong at the same time. While the

local Coulomb repulsion is indeed key, materials aspects turn out to be essential for understanding real correlated materials. In hindsight, we can now put this debate in a different perspective. The electronic many-body problem, in the non-relativistic limit and in the Born-Oppenheimer approximation, is described by the Hamiltonian

$$\hat{H}_e = -\frac{1}{2}\sum_i \nabla_i^2 - \sum_i \sum_\alpha \frac{Z_\alpha}{|\boldsymbol{r}_i - \boldsymbol{R}_\alpha|} + \sum_{i>j} \frac{1}{|\boldsymbol{r}_i - \boldsymbol{r}_j|} + \sum_{\alpha>\alpha'} \frac{Z_\alpha Z_{\alpha'}}{|\boldsymbol{R}_\alpha - \boldsymbol{R}_{\alpha'}|}, \tag{1}$$

where $\{\boldsymbol{r}_i\}$ are electron coordinates, $\{\boldsymbol{R}_\alpha\}$ nuclear coordinates and Z_α the nuclear charges. Using a complete one-electron basis, for example the basis $\{\varphi_a(\boldsymbol{r})\}$, where $\{a\}$ are the quantum numbers, we can write this Hamiltonian in second quantization as

$$\hat{H}_e = \underbrace{-\sum_{ab} t_{ab}\, c_a^\dagger c_b}_{\hat{H}_0} + \underbrace{\frac{1}{2}\sum_{aa'bb'} U_{aa'bb'}\; c_a^\dagger c_{a'}^\dagger c_{b'} c_b}_{\hat{H}_U}. \tag{2}$$

Here the hopping integrals are given by

$$t_{ab} = -\int d\mathbf{r}\; \overline{\varphi_a}(\boldsymbol{r}) \left(-\frac{1}{2}\nabla^2 \underbrace{- \sum_\alpha \frac{Z_\alpha}{|\boldsymbol{r} - \boldsymbol{R}_\alpha|}}_{v_{\rm en}(\boldsymbol{r})} \right) \varphi_b(\boldsymbol{r}), \tag{3}$$

while the elements of the Coulomb tensor are

$$U_{aa'bb'} = \int d\mathbf{r}_2 \int d\mathbf{r}_2\; \overline{\varphi_a}(\boldsymbol{r}_1)\, \overline{\varphi_{a'}}(\boldsymbol{r}_2)\; \frac{1}{|\boldsymbol{r}_1 - \boldsymbol{r}_2|}\; \varphi_{b'}(\boldsymbol{r}_2)\, \varphi_b(\boldsymbol{r}_1). \tag{4}$$

In principle, all complete one-electron bases are equivalent. In practice, since, in the general case, we cannot solve the N-electron problem exactly, some bases are better than others. One possible choice for the basis are the Kohn-Sham orbitals, $\{\varphi_a^{\rm KS}(\boldsymbol{r})\}$, obtained, e.g., in the local density approximation (LDA) or its simple extensions.[1] In this case, it is useful to replace the electron-nuclei interaction $v_{\rm en}(\boldsymbol{r})$ with the DFT potential $v_R(\boldsymbol{r})$, which includes in addition the Hartree term $v_{\rm H}(\boldsymbol{r})$ and the (approximate) exchange-correlation potential $v_{\rm xc}(\boldsymbol{r})$

$$v_{\rm R}(\boldsymbol{r}) = v_{\rm en}(\boldsymbol{r}) + \underbrace{\int d\mathbf{r}'\; \frac{n(\boldsymbol{r}')}{|\boldsymbol{r} - \boldsymbol{r}'|}}_{v_{\rm H}(\boldsymbol{r})} + v_{\rm xc}(\boldsymbol{r}) \tag{5}$$

so that

$$\tilde{t}_{ab} = -\int d\mathbf{r}\; \overline{\varphi_a^{\rm KS}}(\boldsymbol{r}) \left(-\frac{1}{2}\nabla^2 + v_{\rm R}(\boldsymbol{r}) \right) \varphi_b^{\rm KS}(\boldsymbol{r}). \tag{6}$$

To avoid double counting (DC), we have, however, to subtract from $\hat{H}_U$ the term $\hat{H}_{\rm DC}$, which describes the Coulomb terms already included in the hopping integrals

$$\hat{H}_e = \underbrace{-\sum_{ab} \tilde{t}_{ab}\, c_a^\dagger c_b}_{\hat{H}_0 = \hat{H}_e^{\rm LDA}} + \underbrace{\frac{1}{2}\sum_{aba'b'} \tilde{U}_{aa'bb'}\; c_a^\dagger c_{a'}^\dagger c_{b'} c_b - \hat{H}_{\rm DC}}_{\Delta \hat{H}_U}. \tag{7}$$

[1] For the purpose of many-body calculations the differences between LDA, GGA or their simple extensions are in practice negligible; for simplicity, in the rest of the lecture, we thus adopt LDA as representative functional.

For weakly-correlated systems, in the Kohn-Sham basis, the effects included in $\Delta\hat{H}_U$ can, in first approximation, either be neglected or treated as a perturbation. This implies that $\hat{H}_e^{\rm LDA} \sim \hat{H}_{\rm eff}$, where $\hat{H}_{\rm eff}$ is the effective model which provides a good description of the system (at least) at low energy, and which describes emergent effective "elementary particles" and their interactions. Hypothetically, one could imagine that $\hat{H}_{\rm eff}$ is obtained via a canonical transformation, so that $\hat{H}_{\rm eff} \sim \hat{S}^{-1}\hat{H}_e\,\hat{S}$, although the exact form of the operator $\hat{S}$ is unknown.
A defining feature of strong-correlation effects is that they cannot be described via a single-electron Hamiltonian, however. A model of form $\hat{H}_e^{\rm LDA}$ does not describe correctly the Mott metal-insulator transition, no matter what the specific values of the parameters $\tilde{t}_{ab}$ are.[2] Thus for strongly-correlated systems the low-energy effective model must have a different form. For Mott systems a canonical Hamiltonian is the Hubbard model

$$\hat{H} = -\sum_{\sigma}\sum_{ii'} t^{i,i'} c^{\dagger}_{i\sigma} c_{i'\sigma} + U\sum_{i} \hat{n}_{i\uparrow}\hat{n}_{i\downarrow}, \tag{8}$$

which includes, in addition to a single-electron term, the on-site Coulomb repulsion. This Hamiltonian captures the essence of the Mott transition. At half filling, for $U = 0$ it describes a paramagnetic metal, and for $t^{i,i'}(1-\delta_{i,i'})=0$ an insulating set of paramagnetic atoms. Unfortunately, differently from Hamiltonians of type $\hat{H}_e^{\rm LDA}$, Hubbard-like models cannot be solved exactly in the general case. Remarkably, till 30 years ago, no method for describing the complete phase diagram of (8) in one coherent framework, including the paramagnetic insulating phase, was actually known. This changed between 1989 and 1992, when the dynamical mean-field theory (DMFT) was developed [4–7]. The key idea of DMFT consists in mapping the Hubbard model onto a self-consistent *auxiliary quantum-impurity problem*, which can be solved exactly. The mapping is based on the *local dynamical self-energy approximation*, very good for realistic three-dimensional lattices—and becoming exact in the infinite coordination limit [4, 5].
DMFT was initially applied to simple cases, due to limitations in model building, computational power, and numerical methods for solving the auxiliary impurity problem (the quantum impurity solvers). In the last thirty years remarkable progress lifted many of these limitations. First, reliable schemes to build realistic low-energy materials-specific Hubbard-like models have been devised, in particular using Kohn-Sham localized Wannier functions. This is impressive, given that we do not know the exact operator $\hat{S}$ which gives the effective low-energy Hamiltonian, and thus a truly systematic derivation is not possible. Second, key advances in quantum impurity solvers and increasingly more powerful supercomputers made it possible to study always more complex many-body Hamiltonians. The approach which emerged, consisting in solving within DMFT materials-specific many-body Hamiltonians constructed via LDA, is known as the LDA+DMFT method [8–10]. This technique (and its extensions) is now the state-of-the-art for describing strongly-correlated materials. In this lecture I will outline the basic ideas on which the method is based, its successes and its limitations.

[2] One can obtain an insulator by reducing the symmetry, e.g, by increasing the size of the primitive cell. This Slater-type insulator has however different properties than a Mott-type insulator.

2 From DMFT to LDA+DMFT

In this section we introduce the basics of dynamical mean-field theory. We start from a case for which we can perform analytic calculations, the two-site Hubbard Hamiltonian. This is a toy model; it is also the worst case for DMFT, since the coordination number is the lowest possible. It is nonetheless very useful in order to explain how the method works. Next we extend the formalism to the one-band and then to the multi-orbital Hubbard Hamiltonian. For three-dimensional lattices the coordination number is typically large and thus DMFT is an excellent approximation. In Sec. 3 we describe state-of-the-art schemes to construct materials-specific many-body models. They are based on Kohn-Sham Wannier orbitals, calculated, e.g, using the LDA functional. The solution of such models via DMFT defines the LDA+DMFT method.

2.1 DMFT for a toy model: The Hubbard dimer

The two-site Hubbard model is given by

$$\hat{H} = \varepsilon_d \sum_{i\sigma} \hat{n}_{i\sigma} - t \sum_{\sigma} \left(c^\dagger_{1\sigma} c_{2\sigma} + c^\dagger_{2\sigma} c_{1\sigma} \right) + U \sum_i \hat{n}_{i\uparrow} \hat{n}_{i\downarrow}, \tag{9}$$

with $i = 1, 2$. The ground state for $N = 2$ electrons (half filling) is the singlet[3]

$$|G\rangle_H = \frac{a_2(t,U)}{\sqrt{2}} \left(c^\dagger_{1\uparrow} c^\dagger_{2\downarrow} - c^\dagger_{1\downarrow} c^\dagger_{2\uparrow} \right) |0\rangle + \frac{a_1(t,U)}{\sqrt{2}} \left(c^\dagger_{1\uparrow} c^\dagger_{1\downarrow} + c^\dagger_{2\uparrow} c^\dagger_{2\downarrow} \right) |0\rangle \tag{10}$$

with

$$a_1^2(t,U) = \frac{1}{\Delta(t,U)} \frac{\Delta(t,U) - U}{2}, \qquad a_2^2(t,U) = \frac{4t^2}{\Delta(t,U)} \frac{2}{\Delta(t,U) - U}, \tag{11}$$

and

$$\Delta(t,U) = \sqrt{U^2 + 16t^2}. \tag{12}$$

The energy of this state is

$$E_0(2) = 2\varepsilon_d + \frac{1}{2} \left(U - \Delta(t,U) \right). \tag{13}$$

In the $T \to 0$ limit, using the Lehmann representation (see Appendix B), one can show that the local Matsubara Green function for spin σ takes then the form

$$\begin{aligned} G^\sigma_{i,i}(i\nu_n) = \frac{1}{4} \Bigg(& \frac{1 + w(t,U)}{i\nu_n - \big(\underbrace{E_0(2) - \varepsilon_d + t - \mu}_{E_0(2) - E_-(1) - \mu} \big)} + \frac{1 - w(t,U)}{i\nu_n - \big(\underbrace{-E_0(2) + U + 3\varepsilon_d + t - \mu}_{E_+(3) - E_0(2) - \mu} \big)} \\ & + \frac{1 - w(t,U)}{i\nu_n - \big(\underbrace{E_0(2) - \varepsilon_d - t - \mu}_{E_0(2) - E_+(1) - \mu} \big)} + \frac{1 + w(t,U)}{i\nu_n - \big(\underbrace{-E_0(2) + U + 3\varepsilon_d - t - \mu}_{E_-(3) - E_0(2) - \mu} \big)} \Bigg), \end{aligned} \tag{14}$$

[3] Eigenstates and eigenvalues of the Hubbard dimer for arbitrary filling can be found in Appendix A.

where $\nu_n = \pi(2n+1)/\beta$ are fermionic Matsubara frequencies and $\mu = \varepsilon_d + U/2$ is the chemical potential. The weights are

$$w_\pm(t,U) = \frac{1}{4}\big(1 \pm w(t,U)\big), \tag{15}$$

$$w(t,U) = 2a_1(t,U)a_2(t,U) = \frac{4t}{\Delta(t,U)}\,. \tag{16}$$

The local Green function can be rewritten as the average of the Green function for the bonding ($k=0$) and the anti-bonding state ($k=\pi$), i.e.,

$$G^\sigma_{i,i}(i\nu_n) = \frac{1}{2}\Bigg(\underbrace{\frac{1}{i\nu_n + \mu - \varepsilon_d + t - \Sigma^\sigma(0;i\nu_n)}}_{G^\sigma(0;i\nu_n)} + \underbrace{\frac{1}{i\nu_n + \mu - \varepsilon_d - t - \Sigma^\sigma(\pi;i\nu_n)}}_{G^\sigma(\pi;i\nu_n)}\Bigg). \tag{17}$$

The self-energy is given by

$$\Sigma^\sigma(k;i\nu_n) = \frac{U}{2} + \frac{U^2}{4}\frac{1}{i\nu_n + \mu - \varepsilon_d - \frac{U}{2} - \; e^{ik}\; 3t}\,. \tag{18}$$

The self-energies $\Sigma^\sigma(0;i\nu_n)$ and $\Sigma^\sigma(\pi;i\nu_n)$ differ due to the phase $e^{ik} = \pm 1$ in their denominators. The local self-energy is, by definition, the average of the two

$$\begin{aligned}\Sigma^\sigma_l(i\nu_n) = \frac{1}{2}\Big(\Sigma^\sigma(\pi;i\nu_n) + \Sigma^\sigma(0;i\nu_n)\Big) &= \frac{U}{2} + \frac{U^2}{4}\,\frac{i\nu_n + \mu - \varepsilon_d - \frac{U}{2}}{(i\nu_n + \mu - \varepsilon_d - \frac{U}{2})^2 - (3t)^2} \\ &= \frac{U}{2} + \frac{U^2}{4}\,\frac{i\nu_n}{(i\nu_n)^2 - (3t)^2}\end{aligned} \tag{19}$$

The difference

$$\begin{aligned}\Delta\Sigma^\sigma_l(i\nu_n) = \frac{1}{2}\Big(\Sigma^\sigma(\pi;i\nu_n) - \Sigma^\sigma(0;i\nu_n)\Big) &= \frac{U^2}{4}\,\frac{3t}{(i\nu_n + \mu - \varepsilon_d - \frac{U}{2})^2 - (3t)^2} \\ &= \frac{U^2}{4}\,\frac{3t}{(i\nu_n)^2 - (3t)^2},\end{aligned} \tag{20}$$

thus measures the importance of non-local effects; it would be zero if the self-energy was independent of k. Next we define the hybridization function

$$F^\sigma(i\nu_n) = \frac{\big(t + \Delta\Sigma^\sigma_l(i\nu_n)\big)^2}{i\nu_n + \mu - \varepsilon_d - \Sigma^\sigma_l(i\nu_n)} \tag{21}$$

which for $U = 0$ becomes

$$F^\sigma_0(i\nu_n) = \frac{t^2}{i\nu_n}. \tag{22}$$

By using these definitions, we can rewrite the local Green function as

$$G^\sigma_{i,i}(i\nu_n) = \frac{1}{i\nu_n + \mu - \varepsilon_d - F^\sigma(i\nu_n) - \Sigma^\sigma_l(i\nu_n)}. \tag{23}$$

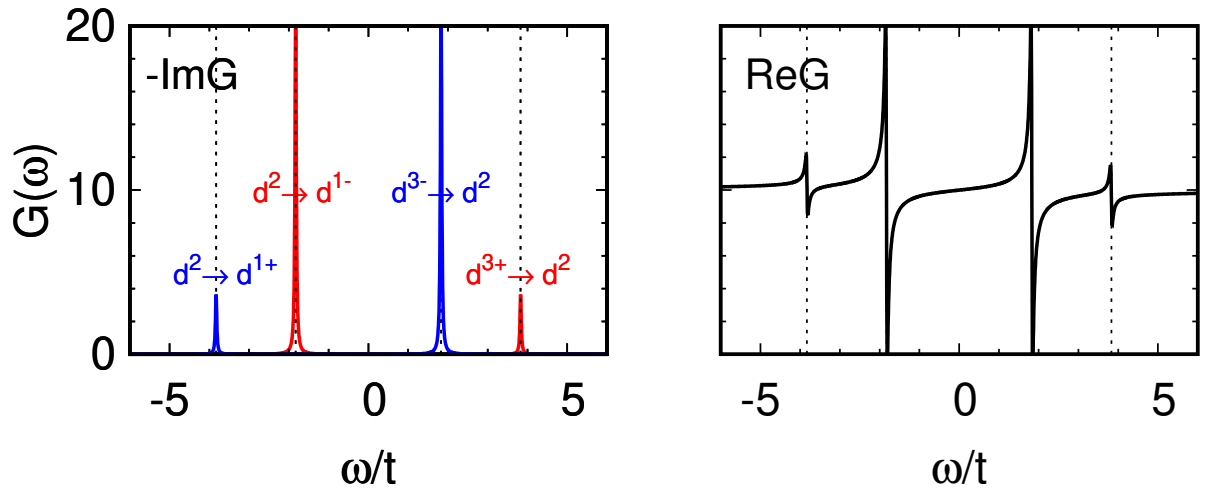

Fig. 1: *Hubbard dimer: Imaginary (left) and real (right) part of the retarded Green function, obtained setting $i\nu_n \to \omega + i\delta$ (analytic continuation) in Eq. (14). Red lines: $k = 0$ contribution. Blue lines: $k = \pi$ contribution. Dashed lines: Poles of the retarded Green function. Parameters: $t = 1, U = 4$. The weight of the poles yielding the smaller peaks, $w_-(t, U)$, defined in Eq. (15), goes to zero for $U \to 0$. In the atomic limit, instead, all four poles have the same weight; the energies of the two positive (negative) poles become identical, however.*

The associated retarded Green function, obtained via analytic continuation ($i\nu_n \to \omega + i\delta$), is shown in Fig. 1. It is important to point out that, as one may see from the formulas just discussed, the local Green function and the local self-energy satisfy the *local Dyson equation*

$$\Sigma_l^\sigma(i\nu_n) = \frac{1}{\mathfrak{G}_{i,i}^\sigma(i\nu_n)} - \frac{1}{G_{i,i}^\sigma(i\nu_n)}\,, \tag{24}$$

where $\mathfrak{G}_{i,i}^\sigma(i\nu_n)$ is given by

$$\mathfrak{G}_{i,i}^\sigma(i\nu_n) = \frac{1}{i\nu_n + \mu - \varepsilon_d - F^\sigma(i\nu_n)}\,. \tag{25}$$

Thus, one could think of mapping the Hubbard dimer into an auxiliary quantum-impurity model, chosen such that, within certain approximations, the impurity Green function is as close as possible to the local Green function of the original problem. How can we do this? Let us adopt as auxiliary model the Anderson molecule

$$\hat{H}^{\mathrm{A}} = \varepsilon_s \sum_\sigma \hat{n}_{s\sigma} - t \sum_\sigma \left(c_{d\sigma}^\dagger c_{s\sigma} + c_{s\sigma}^\dagger c_{d\sigma} \right) + \varepsilon_d \sum_\sigma \hat{n}_{d\sigma} + U \hat{n}_{d\uparrow} \hat{n}_{d\downarrow}, \tag{26}$$

where s labels the uncorrelated bath site and d the correlated quantum-impurity site. The first constraint would be that Hamiltonian (26) has a ground state with the same occupations of the 2-site Hubbard model, i.e., at half filling, $n_d = n_s = 1$. Such a *self-consistency condition* is satisfied if $\varepsilon_s = \mu = \varepsilon_d + U/2$. This can be understood by comparing the Hamiltonian matrices of the two models in the Hilbert space with $N = 2$ electrons. To this end, we first order the

two-electron states of the Hubbard dimer as

$$
\begin{aligned}
|1\rangle &= c^\dagger_{1\uparrow}c^\dagger_{2\uparrow}|0\rangle, & |4\rangle &= \tfrac{1}{\sqrt{2}}\big(c^\dagger_{1\uparrow}c^\dagger_{2\downarrow} - c^\dagger_{1\downarrow}c^\dagger_{2\uparrow}\big)|0\rangle,\\
|2\rangle &= c^\dagger_{1\downarrow}c^\dagger_{2\downarrow}|0\rangle, & |5\rangle &= c^\dagger_{1\uparrow}c^\dagger_{1\downarrow}|0\rangle,\\
|3\rangle &= \tfrac{1}{\sqrt{2}}\big(c^\dagger_{1\uparrow}c^\dagger_{2\downarrow} + c^\dagger_{1\downarrow}c^\dagger_{2\uparrow}\big)|0\rangle, & |6\rangle &= c^\dagger_{2\uparrow}c^\dagger_{2\downarrow}|0\rangle.
\end{aligned}
\tag{27}
$$

In this basis the Hamiltonian of the Hubbard dimer has the matrix form

$$
\hat{H}_2(\varepsilon_d, U, t) = \begin{pmatrix}
2\varepsilon_d & 0 & 0 & 0 & 0 & 0\\
0 & 2\varepsilon_d & 0 & 0 & 0 & 0\\
0 & 0 & 2\varepsilon_d & 0 & 0 & 0\\
0 & 0 & 0 & 2\varepsilon_d & -\sqrt{2}t & -\sqrt{2}t\\
0 & 0 & 0 & -\sqrt{2}t & 2\varepsilon_d{+}U & 0\\
0 & 0 & 0 & -\sqrt{2}t & 0 & 2\varepsilon_d{+}U
\end{pmatrix}. \tag{28}
$$

The ground state, the singlet given in Eq. (10), can be obtained by diagonalizing the lower 3×3 block. For the Anderson molecule, ordering the basis in the same way ($1 \to d, 2 \to s$), this Hamiltonian becomes

$$
\hat{H}^A_2(\varepsilon_d, U, t; \varepsilon_s) = \begin{pmatrix}
\varepsilon_d{+}\varepsilon_s & 0 & 0 & 0 & 0 & 0\\
0 & \varepsilon_d{+}\varepsilon_s & 0 & 0 & 0 & 0\\
0 & 0 & \varepsilon_d{+}\varepsilon_s & 0 & 0 & 0\\
0 & 0 & 0 & \varepsilon_d{+}\varepsilon_s & -\sqrt{2}t & -\sqrt{2}t\\
0 & 0 & 0 & -\sqrt{2}t & 2\varepsilon_d{+}U & 0\\
0 & 0 & 0 & -\sqrt{2}t & 0 & 2\varepsilon_s
\end{pmatrix}. \tag{29}
$$

Comparing the lower 3×3 block of $\hat{H}^A_2(\varepsilon_d, U, t; \varepsilon_s)$ with the corresponding block of $\hat{H}_2(\varepsilon_d, U, t)$ we can see that, unless $\varepsilon_s = \mu = \varepsilon_d + U/2$, the two doubly occupied states $|5\rangle$ and $|6\rangle$ have different energies and thus the two sites $i = 1, 2$ are differently occupied in the ground state. By setting $\varepsilon_s = \mu$ we find that

$$
\hat{H}^A_2(\varepsilon_d, U, t; \mu) = \hat{H}_2(\varepsilon_d{+}\tfrac{U}{4}, \tfrac{U}{2}, t). \tag{30}
$$

The $N = 2$ ground state of $\hat{H}^A_2(\varepsilon_d, U, t; \mu)$ has thus the form of the ground-state for the Hubbard dimer

$$
|G\rangle_A = \frac{a_2(t, U/2)}{\sqrt{2}}\big(c^\dagger_{d\uparrow}c^\dagger_{s\downarrow} - c^\dagger_{d\downarrow}c^\dagger_{s\uparrow}\big)|0\rangle + \frac{a_1(t, U/2)}{\sqrt{2}}\big(c^\dagger_{d\uparrow}c^\dagger_{d\downarrow} + c^\dagger_{s\uparrow}c^\dagger_{s\downarrow}\big)|0\rangle, \tag{31}
$$

and the condition $n_s = n_d = 1$ is satisfied. Since $\varepsilon_s \neq \varepsilon_d$, however, the eigenstates of $\hat{H}^{\rm A}$ for one electron ($N = 1$) or one hole ($N = 3$) are not the bonding and antibonding states of the

Hubbard dimer.[4] The impurity Green function is then given by

$$G^{\sigma}_{d,d}(i\nu_n) = \frac{1}{4}\Bigg(\frac{1+w'(t,U)}{i\nu_n - \big(E_0(2) - E_-(1) - \mu\big)} + \frac{1-w'(t,U)}{i\nu_n - \big(E_+(3) - E_0(2) - \mu\big)} \\ \frac{1-w'(t,U)}{i\nu_n - \big(E_0(2) - E_+(1) - \mu\big)} + \frac{1+w'(t,U)}{i\nu_n - \big(E_-(3) - E_0(2) - \mu\big)}\Bigg), \tag{32}$$

where

$$E_0(2) - E_\pm(1) - \mu = -\Big(E_\pm(3) - E_0(2) - \mu\Big) = -\frac{1}{4}\Big(2\Delta(t,U/2) \pm \Delta(t,U)\Big) \tag{33}$$

and

$$w'(t,U) = \frac{1}{2}\frac{32t^2 - U^2}{\Delta(t,U)\Delta(t,U/2)}\,. \tag{34}$$

After some rearrangement we obtain a much simpler expression

$$G^{\sigma}_{d,d}(i\nu_n) = \frac{1}{i\nu_n + \mu - \varepsilon_d - \mathcal{F}^{\sigma}_0(i\nu_n) - \Sigma^{\sigma}_A(i\nu_n)}\,. \tag{35}$$

The impurity self-energy equals the local self-energy of the Hubbard dimer

$$\Sigma^{\sigma}_A(i\nu_n) = \frac{U}{2} + \frac{U^2}{4}\frac{i\nu_n}{(i\nu_n)^2 - (3t)^2}\,, \tag{36}$$

as one may see comparing it to equation (19). The hybridization function is given by

$$\mathcal{F}^{\sigma}_0(i\nu_n) = \frac{t^2}{i\nu_n}\,, \tag{37}$$

as for the non-interacting Hubbard dimer, Eq. (22). For $U = 0$, $G^{\sigma}_{d,d}(i\nu_n)$ equals the non-interacting impurity Green function

$$G^{0\sigma}_{d,d}(i\nu_n) = \frac{1}{i\nu_n + \mu - \varepsilon_d - \mathcal{F}^{\sigma}_0(i\nu_n)}\,. \tag{38}$$

The impurity Green function thus satisfies the *impurity Dyson equation*

$$\Sigma^{\sigma}_A(i\nu_n) = \frac{1}{G^{0\sigma}_{d,d}(i\nu_n)} - \frac{1}{G^{\sigma}_{d,d}(i\nu_n)}\,. \tag{39}$$

In Fig. 2 we show the retarded impurity Green function of the Anderson molecule (orange, right panels) and the retarded local Green function of the 2-site Hubbard model, both in the local self-energy approximation (blue, right panels) and exact (blue, left panels). Comparing left and right panels we can see that setting $\Delta\Sigma^{\sigma}_l(\omega) = 0$ yields large errors. The right panels demonstrate, however, that the spectral function of the Anderson molecule is quite similar to the

[4]The complete list of eigenvalues and eigenvectors of the Anderson molecule for $\varepsilon_s = \varepsilon_d + U/2$ and arbitrary electron number N can be found in Appendix A.

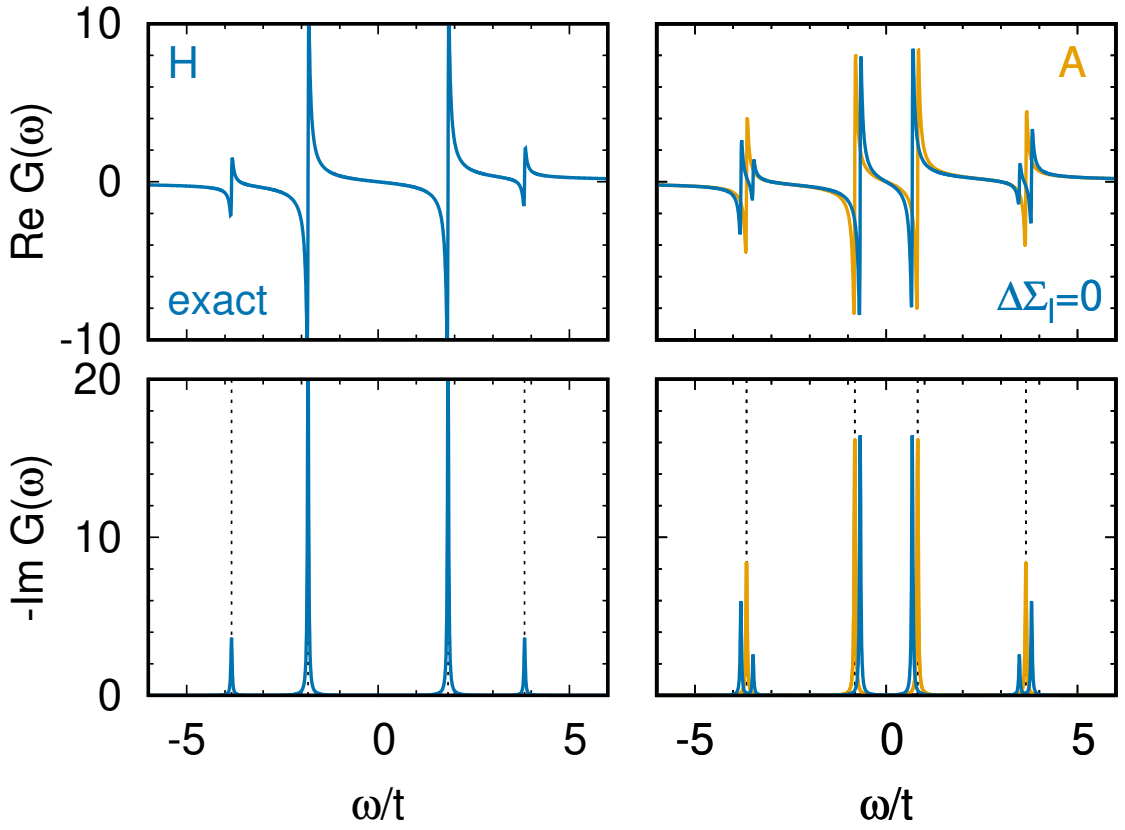

Fig. 2: *Retarded Green function of the Hubbard dimer ($t = 1, U = 4$) and of the Anderson molecule ($\varepsilon_s = \varepsilon_d + U/2$) in the zero temperature limit. Left panels: Hubbard dimer, exact Green function. Right panels, blue: Hubbard dimer in the local self-energy approximation, i.e., with $\Delta\Sigma_l^\sigma(\omega) = 0$. Right panels, orange: Anderson molecule. Dashed lines: Poles for the Hubbard dimer (left) or the Anderson molecule (right).*

one of the Hubbard dimer with $\Delta\Sigma_l^\sigma(\omega) = 0$. The small remaining deviations come from the fact that, for the Hubbard dimer, in the impurity Dyson equation, the non-interacting impurity Green function is replaced by $\mathfrak{G}_{i,i}^\sigma(i\nu_n)$ in the local self-energy approximation, i.e., by the *bath* Green function

$$\mathcal{G}_{i,i}^\sigma(i\nu_n) = \frac{1}{i\nu_n + \mu - \varepsilon_d - \mathcal{F}_l^\sigma(i\nu_n)}\,, \tag{40}$$

where

$$\mathcal{F}_l^\sigma(i\nu_n) = \frac{t^2}{i\nu_n + \mu - \varepsilon_d - \Sigma_A^\sigma(i\nu_n)}\,. \tag{41}$$

We are now in the position of explaining how DMFT works for the Hamiltonian of the Hubbard dimer, choosing the Anderson molecule Hamiltonian (26) as the auxiliary quantum-impurity model. The procedure can be split in the following steps

1. Build the initial quantum impurity model with $G_{d,d}^{0\sigma}(i\nu_n) = G_{i,i}^{0\sigma}(i\nu_n)$. The initial bath is thus defined by energy $\varepsilon_s = \varepsilon_d$ and hopping t.

2. Calculate the local Green function $G^{\sigma}_{d,d}(i\nu_n)$ for the auxiliary model.

3. Use the local Dyson equation to calculate the impurity self-energy

$$\Sigma^{\sigma}_{A}(i\nu_n) = \frac{1}{G^{0\sigma}_{d,d}(i\nu_n)} - \frac{1}{G^{\sigma}_{d,d}(i\nu_n)} \, .$$

4. Calculate the local Green function of the Hubbard dimer setting the self-energy equal to the one of the quantum-impurity model

$$G^{\sigma}_{i,i}(i\nu_n) \sim \frac{1}{2}\left(\frac{1}{i\nu_n + \mu - \varepsilon_d + t - \Sigma^{\sigma}_{A}(i\nu_n)} + \frac{1}{i\nu_n + \mu - \varepsilon_d - t - \Sigma^{\sigma}_{A}(i\nu_n)} \right) .$$

5. Calculate a new bath Green function $\mathcal{G}^{\sigma}_{i,i}(i\nu_n)$ from the local Dyson equation

$$\mathcal{G}^{\sigma}_{i,i}(i\nu_n) = \frac{1}{\Sigma^{\sigma}_{A}(i\nu_n) + 1/G^{\sigma}_{i,i}(i\nu_n)} \, .$$

6. Build a new $G^{0\sigma}_{d,d}(i\nu_n)$ from $\mathcal{G}^{\sigma}_{i,i}(i\nu_n)$.

7. Restart from the second step.

8. Iterate till self-consistency, i.e., here till $n^{\sigma}_{d} = n^{\sigma}_{i}$ and $\Sigma^{\sigma}_{A}(i\nu_n)$ does not change any more.

The Anderson molecule satisfies the self-consistency requirements for $\varepsilon_s = \mu$. The remaining difference between $G^{\sigma}_{d,d}(i\nu_n)$, the impurity Green function, and $G^{\sigma}_{i,i}(i\nu_n)$, the local Green function of the Hubbard dimer in the local self-energy approximation, arises from the difference in the associated hybridization functions

$$\Delta\mathcal{F}_l(i\nu_n) = \mathcal{F}^{\sigma}_{l}(i\nu_n) - \mathcal{F}^{\sigma}_{0}(i\nu_n) = t^2 p^2 \left(-\frac{2}{i\nu_n} + \frac{1}{i\nu_n - \varepsilon_a} + \frac{1}{i\nu_n + \varepsilon_a} \right) \tag{42}$$

where $p^2 = U^2/8\varepsilon_a^2$ and $\varepsilon_a = \sqrt{9t^2 + U^2/4}$. The error made is small, however, as shown in the right panels of Fig. 2. To further improve we would have to modify the auxiliary model adding more bath sites. Staying with the Anderson molecule, in Fig. 3 we compare in more detail its spectral function with the exact spectral function of the Hubbard dimer. The figure emphasizes several important conclusions. The top right panel reminds us that DMFT is not a good approximation for molecular complexes with two (or few) correlated sites. This is because in such systems the coordination number is the lowest possible, the worst case for dynamical mean-field theory. In three-dimensional crystals, instead, the coordination number is typically large enough to make dynamical mean-field theory an excellent approximation. The bottom left panel of Fig. 3 shows that, in the local-self-energy approximation, the agreement between Anderson and Hubbard Green functions is very good for any U value. This indicates that when the local-self-energy approximation (hence DMFT) works well, as in the case of three-dimensional crystals, it can be successfully used to study the behavior of a given system as a function of U. Leaving for a moment DMFT aside, the two bottom panels of Fig. 3 show that

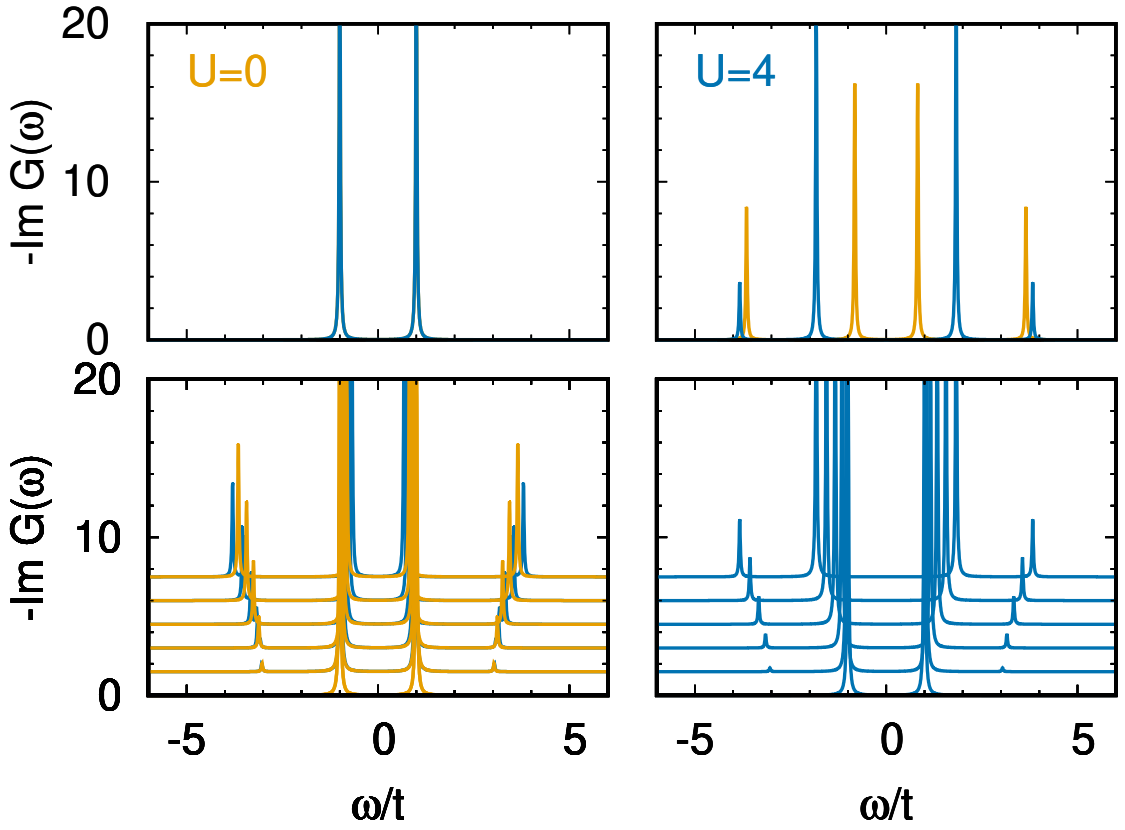

Fig. 3: *Imaginary part of the retarded Green function of the Anderson molecule (orange) and Hubbard dimer (blue) in the zero temperature limit. In the bottom left panel the local self-energy approximation is adopted for the Hubbard dimer; in all other cases the exact Green function of the Hubbard dimer is shown. Parameters:* $t = 1$, $\varepsilon_s = \mu$. *Top:* $U = 0$ *(left) and* $U = 4t$ *(right). Bottom: Evolution with increasing* U *from* 0 *to* $4t$ *in equal steps.*

the evolution with U is different for the impurity Green function of the Anderson molecule and the exact local Green function of the Hubbard dimer. Anticipating the discussion of later sections, if we compare to the spectral function of the actual *lattice* Hubbard model, we could say that the Hubbard dimer captures well the evolution of the Hubbard bands and the gap in the large-U limit. On the other hand, the Anderson molecule partially captures the behavior of the central "quasi-particle" or "Kondo" peak, although the Kondo effect itself is unrealistically described; as a matter of fact, the Kondo energy gain (the "Kondo temperature") is perturbative ($\propto t^2/U$) in the case of the Anderson molecule, while it is exponentially small for a Kondo impurity in a metallic bath. This also points to the possible shortcomings of calculations in which the DMFT quantum-impurity model for the *lattice* Hubbard model is solved via exact diagonalization, however using a single bath site or very few; this is sufficient in the limit of large gap,[5] but is bound to eventually fail approaching the metallic regime. Indeed, this failure is one of the reasons why the solution of the Kondo problem required the development of—at the time new—non-perturbative techniques such as the numerical renormalization group.

[5]For a discussion of bath parametrization in exact diagonalization and the actual convergence with the number of bath sites for the lattice Hubbard model see Ref. [11].

2.2 Non-local Coulomb interaction

In Sec. 2.1 we have seen that the local Coulomb interaction gives rise, *alone*, to non-local self-energy terms, which can be very important. What is, instead, the effect of the non-local part of the Coulomb interaction? For a Hubbard dimer, extending the Coulomb interaction to first neighbors leads to the Hamiltonian

$$\begin{aligned}\hat{H} =& \varepsilon_d \sum_{i\sigma} \hat{n}_{i\sigma} - t \sum_{\sigma} \left(c^\dagger_{1\sigma} c_{2\sigma} + c^\dagger_{2\sigma} c_{1\sigma}\right) + U \sum_{i=1,2} \hat{n}_{i\uparrow}\hat{n}_{i\downarrow} \\ &+ \sum_{\sigma\sigma'} \left(V - 2J_V - J_V\,\delta_{\sigma\sigma'}\right) \hat{n}_{1\sigma}\hat{n}_{2\sigma'} - J_V \sum_{i\neq i'} \left(c^\dagger_{i\uparrow} c_{i\downarrow} c^\dagger_{i'\downarrow} c_{i'\uparrow} + c^\dagger_{i'\uparrow} c^\dagger_{i'\downarrow} c_{i\uparrow} c_{i\downarrow}\right), \end{aligned} \tag{43}$$

where the parameters in the last two terms are the intersite direct (V) and exchange (J_V) Coulomb interaction. For two electrons the Hamiltonian, in a matrix form, becomes

$$\hat{H}_2^{\rm NL} = \begin{pmatrix} 2\varepsilon_d{+}V{-}3J_V & 0 & 0 & 0 & 0 & 0 \\ 0 & 2\varepsilon_d{+}V{-}3J_V & 0 & 0 & 0 & 0 \\ 0 & 0 & 2\varepsilon_d{+}V{-}3J_V & 0 & 0 & 0 \\ 0 & 0 & 0 & 2\varepsilon_d{+}V{-}J_V & -\sqrt{2}t & -\sqrt{2}t \\ 0 & 0 & 0 & -\sqrt{2}t & 2\varepsilon_d{+}U & -J_V \\ 0 & 0 & 0 & -\sqrt{2}t & -J_V & 2\varepsilon_d{+}U \end{pmatrix},$$

where the basis is defined in Eq. (27). In the atomic ($t = 0$) limit, the triplet states, $|1\rangle$, $|2\rangle$ and $|3\rangle$, have lower energy than the singlet states, $|4\rangle$, $|5\rangle$ and $|6\rangle$, as one can see by comparing the diagonal elements of the upper and lower 3×3 block of the matrix $\hat{H}_2^{\rm NL}$ here above. This is due to the fact that J_V is positive (ferromagnetic) and $V < U$. The triplet can remain the ground multiplet even for finite t. If, however, J_V is sufficiently small, the ground state is a singlet, as in the case $V{=}J_V{=}0$. Setting for simplicity $J_V = 0$, we notice that $\hat{H}_2^{\rm NL} = \hat{H}_2(\varepsilon'_d, U', t)$, where the right-hand-side term is the $N{=}2$-electron Hamiltonian of the $J_V{=}V{=}0$ Hubbard dimer, Eq. (28), with parameters $\varepsilon'_d = \varepsilon_d + V/2$ and $U'{=}U{-}V$. The $N{=}2$ ground state is thus still given by Eq. (10), provided that we replace U with U' in the coefficients. Eventually, in the limiting case $U{=}V$, $\hat{H}_2^{\rm NL}$ equals the corresponding Hamiltonian of an effective non-correlated dimer, $\hat{H}_2(\varepsilon'_d, 0, t)$. What happens away from half filling? For $N{=}1$ electrons, eigenvectors and eigenvalues are the same as in the $V{=}0$ case; for $N{=}3$ electrons all energies are shifted by $2V$. Summarizing, we can obtain the Green function for $V \neq 0$ from Eq. (14) setting

$$\begin{aligned} E_\pm(N{=}1, U; V) &= E_\pm(N{=}1, U; 0) &&= \varepsilon_d \pm t \\ E_\pm(N{=}3, U; V) &= E_\pm(N{=}3, U; 0) + 2V &&= 3\varepsilon_d \pm t + U + 2V \\ E_0(N{=}2, U; V) &= E_0(N{=}2, U{-}V; 0) + V &&= E_0(2, U{-}V) + V \\ \mu(U; V) &= \mu(U) + V &&= \mu + V \\ w_\pm(t, U; V) &= w_\pm(t, U{-}V; 0). \end{aligned}$$

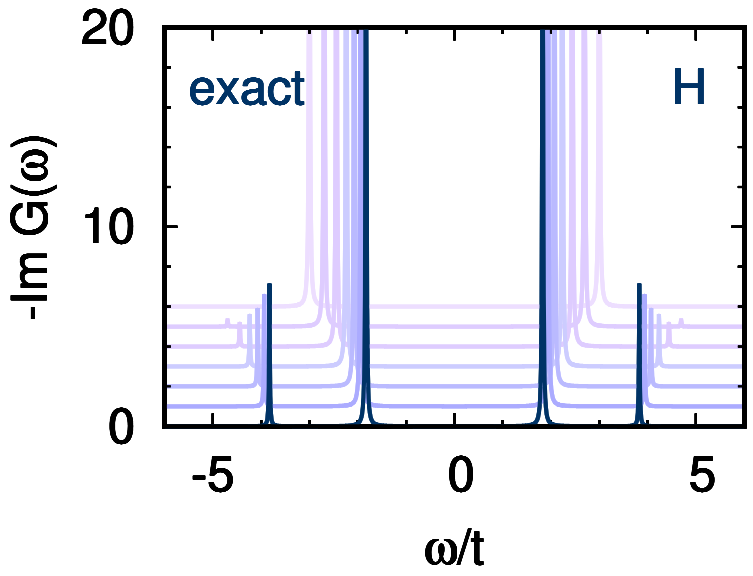

Fig. 4: *Imaginary part of the retarded Green function of the Hubbard dimer in the zero temperature limit ($U = 4$, $t = 1$), increasing the intersite Coulomb repulsion V from 0 to $V = U = 4$ in equal steps; we have set $J_V = 0$. The dark blue line corresponds to $V = 0$.*

Thus we have, recalling that $U' = U - V$,

$$G^{\sigma}_{i,i}(i\nu_n) = \frac{w_+(t,U')}{i\nu_n - \left(E'_0(2) - \frac{1}{2}V - \varepsilon_d + t - \mu'\right)} + \frac{w_-(t,U')}{i\nu_n - \left(-E'_0(2) + U' + \frac{1}{2}V + 3\varepsilon_d + t - \mu'\right)}$$
$$+ \frac{w_-(t,U')}{i\nu_n - \left(E'_0(2) - \frac{1}{2}V - \varepsilon_d - t - \mu'\right)} + \frac{w_+(t,U')}{i\nu_n - \left(-E'_0(2) + U' + \frac{1}{2}V + 3\varepsilon_d - t - \mu'\right)}\,, \qquad (44)$$

where we set $\mu' = \mu - V/2 = 2\varepsilon_d + U'/2$ and $E'_0(2) = E_0(2, U')$. The associated spectral function is shown in Fig. 4. The figure illustrates that increasing V from 0 to U makes the spectra progressively closer to the one of a non-correlated system. Eventually, for $U{=}V$, only two poles contribute, since $w_-(t, U') = 0$. In this limit, the spectral function is identical to the one of the non-interacting Hubbard dimer, however with an enhanced effective hopping, $t \longrightarrow t + V/2$. We can thus say that, in first approximation, the (positive) intersite coupling V effectively reduces the strength of correlations in the Hubbard dimer. In conclusion, the case of the Hubbard dimer explains why *strong-correlation* effects typically appear when the *local term of the electron-electron repulsion dominates*, i.e., when it is much larger than long-range terms. A hypothetical system in which the Coulomb interaction strength is independent on the distance between sites (for the dimer, $U{=}V$) is likely to be already well described via an *effective weakly correlated model*. Of course, in real materials, the effects of long-range Coulomb repulsion can be much more complicated than in the two-site model just discussed, but the general considerations made here remain true even in realistic cases.

2.3 Quantum-impurity solvers: Continuous-time quantum Monte Carlo

For the case of the Anderson molecule exact diagonalization is the simplest quantum-impurity solver and the one that provides most insights. Methods based on quantum Monte Carlo (QMC) sampling are often, however, the only option for realistic multi-orbital and/or multi-site models. Thus, here we explain how to obtain the impurity Green function of the Anderson molecule via hybridization-expansion continuous-time QMC [12], a very successful QMC-based quantum-impurity solver. In this approach, the first step consists in splitting the Hamiltonian into bath ($\hat{H}_{\rm bath}$), hybridization ($\hat{H}_{\rm hyb}$), and local ($\hat{H}_{\rm loc}$) terms

$$\hat{H}^{\rm A} = \underbrace{\varepsilon_s \sum_\sigma \hat{n}_{s\sigma}}_{\hat{H}_{\rm bath}} \underbrace{-t \sum_\sigma \left(c^\dagger_{d\sigma} c_{s\sigma} + c^\dagger_{s\sigma} c_{d\sigma} \right)}_{\hat{H}_{\rm hyb}} + \underbrace{\varepsilon_d \sum_\sigma \hat{n}_{d\sigma} + U \hat{n}_{d\uparrow} \hat{n}_{d\downarrow}}_{\hat{H}_{\rm loc}} . \tag{45}$$

Next, we write the partition function Z as a perturbation series in the hybridization. To this end, we define $\hat{H}_0 = \hat{H}_{\rm bath} + \hat{H}_{\rm loc}$ and rewrite the partition function as

$$Z = {\rm Tr} \left(e^{-\beta(\hat{H}_0 - \mu \hat{N})} \hat{V}(\beta) \right) \tag{46}$$

where the operator $\hat{V}(\beta)$ is given by

$$\hat{V}(\beta) = e^{\beta(\hat{H}_0 - \mu \hat{N})} \, e^{-\beta(\hat{H}_0 + \hat{H}_{\rm hyb} - \mu \hat{N})} = \sum_m \underbrace{\int_0^\beta d\tau_1 \cdots \int_{\tau_{m-1}}^\beta d\tau_m}_{\int d\boldsymbol{\tau}^m} \underbrace{(-1)^m \prod_{l=m}^1 \hat{H}_{\rm hyb}(\tau_l)}_{\hat{O}^m(\boldsymbol{\tau})} , \tag{47}$$

and

$$\hat{H}_{\rm hyb}(\tau_l) = e^{\tau_l(\hat{H}_0 - \mu \hat{N})} \, \hat{H}_{\rm hyb} \, e^{-\tau_l(\hat{H}_0 - \mu \hat{N})} = -t \sum_\sigma \left(c^\dagger_{d\sigma_l}(\tau_l) c_{s\sigma_l}(\tau_l) + c^\dagger_{s\sigma_l}(\tau_l) c_{d\sigma_l}(\tau_l) \right). \tag{48}$$

In this expansion, the only terms that contribute to the trace are even order ones ($m = 2k$) and they are products of impurity (d) and bath (s) creator-annihilator pairs. We can thus rewrite

$$\int d\boldsymbol{\tau}^{2k} \longrightarrow \int d\boldsymbol{\tau}^k \int d\bar{\boldsymbol{\tau}}^k \quad \text{and} \qquad \hat{O}^{2k}(\boldsymbol{\tau}) \longrightarrow \sum_{\boldsymbol{\sigma}, \bar{\boldsymbol{\sigma}}} \hat{O}^{2k}_{\boldsymbol{\sigma}, \bar{\boldsymbol{\sigma}}}(\boldsymbol{\tau}, \bar{\boldsymbol{\tau}}) \tag{49}$$

where

$$\hat{O}^{2k}_{\boldsymbol{\sigma}, \bar{\boldsymbol{\sigma}}}(\boldsymbol{\tau}, \bar{\boldsymbol{\tau}}) = (t)^{2k} \prod_{i=1}^k \left(c^\dagger_{d\bar{\sigma}_i}(\bar{\tau}_i) c_{s\bar{\sigma}_i}(\bar{\tau}_i) c^\dagger_{s\sigma_i}(\tau_i) c_{d\sigma_i}(\tau_i) \right). \tag{50}$$

The vector $\boldsymbol{\sigma} = (\sigma_1, \sigma_2, ..., \sigma_k)$ gives the spins $\{\sigma_i\}$ associated with the k impurity annihilators at imaginary times $\{\tau_i\}$, while $\bar{\boldsymbol{\sigma}} = (\bar{\sigma}_1, \bar{\sigma}_2, ..., \bar{\sigma}_k)$ gives the spins $\{\bar{\sigma}_i\}$ associated with the k impurity creators at imaginary times $\{\bar{\tau}_i\}$. It follows that the local and bath traces can be

decoupled and the partition function can be rewritten as

$$\frac{Z}{Z_{\rm bath}} = \sum_k \int d\boldsymbol{\tau}^k \int d\bar{\boldsymbol{\tau}}^k \sum_{\boldsymbol{\sigma},\bar{\boldsymbol{\sigma}}} d^k_{\bar{\boldsymbol{\sigma}},\boldsymbol{\sigma}}(\boldsymbol{\tau},\bar{\boldsymbol{\tau}})\, t^k_{\boldsymbol{\sigma},\bar{\boldsymbol{\sigma}}}(\boldsymbol{\tau},\bar{\boldsymbol{\tau}}) \tag{51}$$

$$d^k_{\bar{\boldsymbol{\sigma}},\boldsymbol{\sigma}}(\boldsymbol{\tau},\bar{\boldsymbol{\tau}}) = \frac{t^{2k}}{Z_{\rm bath}}\, {\rm Tr}_{\rm bath}\left(e^{-\beta(\hat{H}_{\rm bath}-\mu\hat{N}_s)}\mathcal{T}\prod_{i=k}^1 c^\dagger_{s\sigma_i}(\tau_i)c_{s\bar{\sigma}_i}(\bar{\tau}_i)\right) \tag{52}$$

$$t^k_{\boldsymbol{\sigma},\bar{\boldsymbol{\sigma}}}(\boldsymbol{\tau},\bar{\boldsymbol{\tau}}) = {\rm Tr}_{\rm loc}\left(e^{-\beta(\hat{H}_{\rm loc}-\mu\hat{N}_d)}\mathcal{T}\prod_{i=k}^1 c_{d\sigma_i}(\tau_i)c^\dagger_{d\bar{\sigma}_i}(\bar{\tau}_i)\right), \tag{53}$$

where $Z_{\rm bath} = 1 + 2e^{-\beta(\varepsilon_s-\mu)} + e^{-2\beta(\varepsilon_s-\mu)}$ and

$$c_{d\sigma}(\tau) = e^{\tau(\hat{H}_{\rm loc}-\mu\hat{N}_d)}c_{d\sigma}e^{-\tau(\hat{H}_{\rm loc}-\mu\hat{N}_d)}, \qquad c_{s\sigma}(\tau) = e^{\tau(\hat{H}_{\rm bath}-\mu\hat{N}_s)}c_{s\sigma}e^{-\tau(\hat{H}_{\rm bath}-\mu\hat{N}_s)}.$$

The trace involving only bath operators is simple to calculate, since $\hat{H}_{\rm bath}$ describes an independent-electron problem for which Wick's theorem holds. It is given by the determinant

$$d^k_{\bar{\boldsymbol{\sigma}},\boldsymbol{\sigma}}(\boldsymbol{\tau},\bar{\boldsymbol{\tau}}) = \det\left(\mathcal{F}^k_{\bar{\boldsymbol{\sigma}},\boldsymbol{\sigma}}(\boldsymbol{\tau},\bar{\boldsymbol{\tau}})\right) \tag{54}$$

of the $k\times k$ non-interacting hybridization-function matrix, with elements

$$\left(\mathcal{F}^k_{\bar{\boldsymbol{\sigma}},\boldsymbol{\sigma}}(\boldsymbol{\tau},\bar{\boldsymbol{\tau}})\right)_{i',i} = \mathcal{F}^0_{\bar{\sigma}_{i'},\sigma_i}(\bar{\tau}_{i'}-\tau_i) \tag{55}$$

where

$$\mathcal{F}^0_{\bar{\sigma},\sigma}(\tau) = \delta_{\bar{\sigma},\sigma}\,\frac{t^2}{1+e^{-\beta(\varepsilon_s-\mu)}} \times \begin{cases} -e^{-\tau(\varepsilon_s-\mu)} & \tau>0, \\ +e^{-(\beta+\tau)(\varepsilon_s-\mu)} & \tau<0. \end{cases} \tag{56}$$

This is the imaginary time Fourier transform of the hybridization function introduced previously

$$\mathcal{F}^0_{\bar{\sigma},\sigma}(i\nu_n) = \frac{t^2}{i\nu_n-(\varepsilon_s-\mu)}\,\delta_{\bar{\sigma},\sigma}. \tag{57}$$

The calculation of the local trace is in general more complicated. In the case discussed here, the Hamiltonian does not flip spins. Thus only terms with an equal number of creation and annihilation operators *per spin* contribute to the local trace, and we can express the partition function in expansion orders per spin, k_σ. This yields [13]

$$\frac{Z}{Z_{\rm bath}} = \left(\prod_\sigma \sum_{k_\sigma=0}^\infty \int d\boldsymbol{\tau}_\sigma^{k_\sigma}\int d\bar{\boldsymbol{\tau}}_\sigma^{k_\sigma}\right) d^k_{\bar{\boldsymbol{\sigma}},\boldsymbol{\sigma}}(\boldsymbol{\tau},\bar{\boldsymbol{\tau}})\, t^k_{\boldsymbol{\sigma},\bar{\boldsymbol{\sigma}}}(\boldsymbol{\tau},\bar{\boldsymbol{\tau}}) \tag{58}$$

where the vectors $\boldsymbol{\sigma} = (\boldsymbol{\sigma}_\uparrow,\boldsymbol{\sigma}_\downarrow)$ and $\bar{\boldsymbol{\sigma}} = (\bar{\boldsymbol{\sigma}}_\uparrow,\bar{\boldsymbol{\sigma}}_\downarrow)$ have $(k_\uparrow,k_\downarrow)$ components, and for each k_σ component $\sigma_i = \bar{\sigma}_i = \sigma$. Thus

$$t^k_{\boldsymbol{\sigma},\bar{\boldsymbol{\sigma}}}(\boldsymbol{\tau},\bar{\boldsymbol{\tau}}) = {\rm Tr}_{\rm loc}\left(e^{-\beta(\hat{H}_{\rm loc}-\mu\hat{N}_d)}\,\mathcal{T}\prod\nolimits_\sigma\prod\nolimits_{i=k_\sigma}^1 c_{d\sigma}(\tau_{\sigma_i})c^\dagger_{d\sigma}(\bar{\tau}_{\bar{\sigma}_i})\right). \tag{59}$$

The latter can be calculated analytically. To do this, first we parametrize all configurations for a given spin via a timeline $[0,\beta)$ plus a number of creator/annihilator pairs which define segments

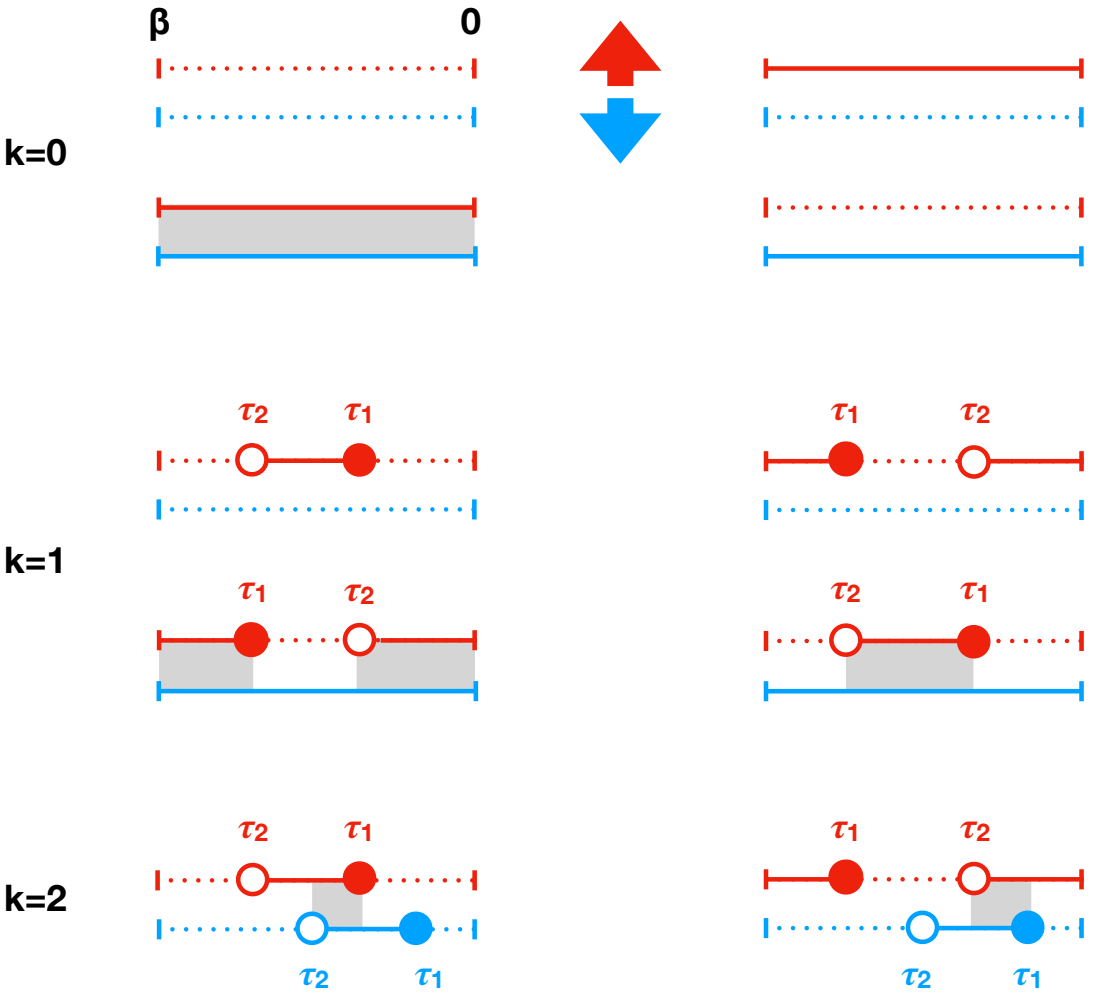

Fig. 5: *Representative configurations contributing to the local trace at zeroth, first and second order. The timelines for spin up are red and those for spin down are blue. The filled circles correspond to the insertion of a creator (time τ_1), and the empty circles to the insertion of an annihilator (time τ_2). Dotted lines represent the vacuum state for a given spin, full lines the occupied state. The grey boxes indicate the regions in which $l_{\uparrow,\downarrow} \neq 0$.*

on the timeline. At zeroth order two possible configurations exist per spin, an empty timeline, which corresponds to the vacuum state $|0\rangle$, and a full timeline, which corresponds to the state $c^\dagger_{d\sigma}|0\rangle$. A given configuration yields, at order $k = k_\uparrow + k_\downarrow$

$$t^k_{\sigma,\bar{\sigma}}(\boldsymbol{\tau},\bar{\boldsymbol{\tau}}) = \left(\prod_\sigma s^{k_\sigma}_\sigma\right) e^{-\sum_{\sigma\sigma'}((\varepsilon_d-\mu)\delta_{\sigma\sigma'}+\frac{U}{2}(1-\delta_{\sigma,\sigma'}))l_{\sigma,\sigma'}} \tag{60}$$

where $l_{\sigma,\sigma'}$ is the length of the overlap of the τ segments for spins σ and σ', respectively, while $s_\sigma = \mathrm{sign}(\tau_{\sigma_1} - \bar{\tau}_{\sigma_1})$ is the fermionic sign. Possible configurations at order $k = 0, 1, 2$ are shown in Fig. 5. At order $k = 0$, summing up the contribution of the four configurations shown in Fig. 5 yields the local partition function $Z_{\mathrm{loc}} = 1 + 2e^{-\beta(\varepsilon_d-\mu)} + e^{-\beta(2(\varepsilon_d-\mu)+U)}$. Order $k = 1$ is already more complicated. Setting $\varepsilon_s = \mu$ as in the self-consistent solution, the contribution

to the bath trace in this case is

$$d^1_{\bar\sigma\sigma}(\tau_1,\tau_2) = \mathcal{F}^0_{\bar\sigma\sigma}(\tau_1,\tau_2) = -\frac{t^2}{2}\delta_{\sigma,\bar\sigma}\ \mathrm{sign}(\tau_1-\tau_2). \tag{61}$$

The local trace at the same order is instead given by

$$t^1_{\sigma\bar\sigma}(\tau_2,\tau_1) = \mathrm{Tr}_{\rm loc}\Big(e^{-\beta(\hat H_{\rm loc}-\mu\hat N_d)}\mathcal{T}c_{d\sigma}(\tau_2)c^\dagger_{d\sigma}(\tau_1)\Big). \tag{62}$$

We can now calculate the contribution at half filling of the four $k=1$ configurations shown in Fig. 5. In the case $k_\uparrow = 1$ and $k_\downarrow = 0$ we have, going from left to right in each row

$$t^1_{\uparrow\uparrow}(\tau_2,\tau_1) = \begin{cases} +e^{-(\tau_2-\tau_1)(\varepsilon_d-\mu)} & = +e^{+\tau_{21}U/2} \\ -e^{-(\beta-(\tau_1-\tau_2))(\varepsilon_d-\mu)} & = -e^{(\beta+\tau_{21})U/2} \\ -e^{-\beta(2(\varepsilon_d-\mu)+U)+(\tau_1-\tau_2)(\varepsilon_d-\mu+U)} & = -e^{-\tau_{21}U/2} \\ +e^{-(\tau_2-\tau_1)(\varepsilon_d-\mu+U)-\beta(\varepsilon_d-\mu)} & = +e^{(\beta-\tau_{21})U/2} \end{cases} \tag{63}$$

where $\tau_{21} = \tau_2 - \tau_1$ and $\mu = \varepsilon_d + U/2$. Similar results can be obtained for $k_\uparrow = 0$ and $k_\downarrow = 1$. Summing up all terms up to order one we find

$$\begin{aligned} \frac{Z}{Z_{\rm bath}} &\sim Z_{\rm loc} + \sum_\sigma \int_0^\beta d\tau_2 \int_0^\beta d\tau_1\, d^1_{\sigma\sigma}(\tau_1,\tau_2)\, t^1_{\sigma\sigma}(\tau_2,\tau_1) \\ &\sim Z_{\rm loc}\left(1 - \beta\,\frac{1-e^{\frac{\beta U}{2}}}{1+e^{\frac{\beta U}{2}}}\frac{2t^2}{U}\right). \end{aligned} \tag{64}$$

The exact formula of the partition function can be obtained from the eigenvalues and eigenvectors in Appendix A

$$\frac{Z}{Z_{\rm bath}} = Z_{\rm loc}\frac{3(1+e^{\frac{\beta U}{2}}) + e^{\frac{\beta U}{4}}\left(4e^{-\frac{\beta\Delta(t,U)}{4}} + 4e^{+\frac{\beta\Delta(t,U)}{4}} + e^{+\frac{\beta\Delta(t,U/2)}{2}} + e^{-\frac{\beta\Delta(t,U/2)}{2}}\right)}{8\big(1+e^{\frac{\beta U}{2}}\big)}. \tag{65}$$

Its Taylor expansion in powers of t/U yields, at second order, the expression above. Going back to Eq. (62), one can observe that, for $k=1$, the local trace is proportional to the local Green function, $G^\sigma_{d,d}(\tau)$. Indeed, $G^\sigma_{d,d}(\tau)$ can be calculated using the configurations just described—provided that we start from $k=1$ and we divide by the hybridization function. More specifically, for $k=1$ and $\tau > 0$ we have

$$G^\sigma_{d,d}(\tau) \sim -\frac{1}{\beta}\int_0^\beta\int_0^\beta \underbrace{d\tau_2 d\tau_1\, d^1_{\sigma\sigma}(\tau_1,\tau_2)t^1_{\sigma\sigma}(\tau_2,\tau_1)}_{w^1}\ \delta\big(\tau-(\tau_2-\tau_1)\big)\ \frac{1}{\mathcal{F}^0_{\sigma\sigma}(\tau_1-\tau_2)}. \tag{66}$$

We are now ready to generalize to arbitrary order. Taking all k values into account, the partition function can be expressed as the sum over all configurations $\{c\}$, i.e., in short

$$Z = \sum_c w_c = \sum_c |w_c|\ \mathrm{sign}\ w_c. \tag{67}$$

In a compact form, we can write $w_c = d\boldsymbol{\tau}_c \; d_c \; t_c$ where $d\boldsymbol{\tau}_c = \prod_\sigma \prod_i^{k_\sigma} d\tau_{\sigma_i} d\bar{\tau}_{\bar{\sigma}_i}$, and d_c and t_c are the bath and local traces for the configuration c. This expression of the partition function shows that we can interpret $|w_c|$ as the sampling weight of configuration c. A generic observable $\hat{O}$ can then be obtained as the Monte Carlo average on a finite number of configurations N_c

$$\langle \hat{O} \rangle = \frac{\sum_c \langle \hat{O} \rangle_c |w_c| \operatorname{sign} w_c}{\sum_c |w_c| \operatorname{sign} w_c} = \frac{\sum_c \operatorname{sign} w_c \langle \hat{O} \rangle_c \, |w_c| / \sum_c |w_c|}{\sum_c \operatorname{sign} w_c \, |w_c| / \sum_c |w_c|} \approx \frac{\frac{1}{N_c} \sum_c^{N_c} \langle \hat{O} \rangle_c \operatorname{sign} w_c}{\frac{1}{N_c} \sum_c \operatorname{sign} w_c}. \quad (68)$$

The term $\frac{1}{N_c} \sum_c \operatorname{sign} w_c$ in the denominator is the average fermionic sign. When this is small, much longer runs are required to obtain data of the same quality; eventually the computational time can become so long that the calculation is unfeasible—in these cases we have a sign problem. In practice, the QMC simulation starts from a random configuration c. Next we propose an update $c \to c'$. Within the Metropolis algorithm, the acceptance ratio is

$$R_{c \to c'} = \min\left(1, \frac{p_{c' \to c}}{p_{c \to c'}} \frac{|w_{c'}|}{|w_c|}\right) \quad (69)$$

where $p_{c \to c'}$ is the proposal probability for the update $c \to c'$. In the approach described here, known as *segment solver*, the basic updates are addition and removal of segments, antisegments (segments winding over the borders of the timeline, see Fig. 5), or complete lines. As example, let us consider the insertion of a segment for spin σ. A segment is made by a creator and an annihilator. The creator is inserted at time τ_{in}; the move is rejected if τ_{in} is in a region where a segment exists. If created, the segment can have at most length $l_{\max}$, given by the distance between τ_{in} and the time at which the next creator is, hence

$$p_{c \to c'} = \frac{d\bar{\tau}}{\beta} \frac{d\tau}{l_{\max}} \, . \quad (70)$$

The proposal probability of the reverse move (removing a segment) is instead given by the inverse of the number of existing segments

$$p_{c' \to c} = \frac{1}{k_\sigma + 1} \, . \quad (71)$$

The acceptance ratio for the insertion of a segment becomes then

$$R_{c \to c'} = \min\left(1, \frac{\beta l_{max}}{k_\sigma + 1} \left| \frac{d_{c'}}{d_c} \frac{t_{c'}}{t_c} \right| \right). \quad (72)$$

For the impurity Green function, here the most important observable, the direct average yields

$$\langle \hat{O} \rangle_c = \langle G^\sigma_{d,d} \rangle_c = \sum_{\sigma'} \sum_{i=1}^{k_\sigma} \sum_{j=1}^{k_\sigma} \Delta(\tau, \tau_{\sigma' j} - \bar{\tau}_{\sigma' j}) \left(M^{k'_\sigma}\right)_{\sigma' j, \sigma' i} \delta_{\sigma, \sigma_{\sigma' j}} \delta_{\sigma, \bar{\sigma}_{\sigma' i}} \quad (73)$$

where $M^k = \left(\mathcal{F}^k\right)^{-1}$ is the inverse of the hybridization matrix and

$$\Delta(\tau, \tau') = -\frac{1}{\beta} \begin{cases} \delta(\tau - \tau') & \tau' > 0 \\ -\delta(\tau - (\tau' + \beta)) & \tau' < 0 \end{cases} . \quad (74)$$

One can verify that at order $k = 1$ this indeed returns Eq. (66).

2.4 Hartree-Fock (LDA+U) versus DMFT approximation

Let us now compare the exact solution of the Hubbard dimer with the result of the Hartree-Fock (HF) approximation, which is the basis of the LDA+U method. It consists in replacing

$$\hat{H}_U = U \sum_i \hat{n}_{i\uparrow}\hat{n}_{i\downarrow} \rightarrow \hat{H}_U^{\rm HF} = U \sum_i \left(\hat{n}_{i\uparrow}\bar{n}_{i\downarrow} + \hat{n}_{i\downarrow}\bar{n}_{i\uparrow} - \bar{n}_{i\uparrow}\bar{n}_{i\downarrow}\right), \tag{75}$$

where $\bar{n}_{i\sigma}$ is the HF expectation value of the operator $\hat{n}_{i\sigma}$. It is convenient to define

$$\begin{aligned} n_i &= \bar{n}_{i\uparrow}+\bar{n}_{i\downarrow} & n &= \frac{1}{2}\left(n_1+n_2\right) & \delta n &= \frac{1}{2}\left(n_1-n_2\right) \\ m_i &= \frac{1}{2}\left(\bar{n}_{i\uparrow}-\bar{n}_{i\downarrow}\right) & m_+ &= \frac{1}{2}\left(m_1+m_2\right) & m_- &= \frac{1}{2}\left(m_1-m_2\right) \end{aligned}$$

Inverting these relations, in the absence of charge disproportionation ($\delta n = 0$), we find

$$\bar{n}_{i\uparrow} = \left(m_+ + (-1)^{i-1} m_-\right) + n/2 \qquad \bar{n}_{i\downarrow} = -\left(m_+ + (-1)^{i-1} m_-\right) + n/2\,.$$

The Hartree-Fock version of the Hubbard dimer Hamiltonian equals the non-interacting Hamiltonian plus a shift of the on-site level. This shift depends on the site and the spin

$$\hat{H}_{\rm HF} = \sum_{i\sigma} \left(\varepsilon_d + \Delta_{i\sigma}\right)\hat{n}_{i\sigma} - t \sum_{\sigma} \left(c^\dagger_{1\sigma} c_{2\sigma} + c^\dagger_{2\sigma} c_{1\sigma}\right) - \Delta_0 \tag{76}$$

$$\Delta_0 = 2U \left(\frac{n^2}{4} - m_+^2 - m_-^2\right) \tag{77}$$

$$\Delta_{i\sigma} = U \left(\frac{1}{2} n - \sigma \left(m_+ + (-1)^{i-1} m_-\right)\right), \tag{78}$$

where $\sigma = +1$ for spin up and $\sigma = -1$ for spin down. Thus we can write immediately the local Green function matrix for site i. It is convenient to use the site basis, hence, to calculate the matrix $G^\sigma_{i,i'}(i\nu_n)$. Then we have

$$G^\sigma_{i,i}(i\nu_n) = \begin{pmatrix} i\nu_n - \left(\varepsilon_d - \mu + \Sigma^\sigma_{1,1}(i\nu_n)\right) & t \\ t & i\nu_n - \left(\varepsilon_d - \mu + \Sigma^\sigma_{2,2}(i\nu_n)\right) \end{pmatrix}^{-1}_{i,i} \tag{79}$$

where we introduced the diagonal self-energy matrix $\Sigma^\sigma_{i,i'}(i\nu_n) = \Delta_{i\sigma}\,\delta_{i,i'}$. This shows that the Hartree-Fock self-energy is not dependent on the frequency, i.e., Hartree-Fock is a *static* mean-field approach. The value of the parameters m_+ and m_- have to be found solving the *self-consistent equations*

$$\bar{n}_{i\sigma} = \langle \hat{n}_{i\sigma} \rangle = \frac{1}{\beta} \sum_n e^{-i\nu_n 0^-} G^\sigma_{i,i}(i\nu_n) = G^\sigma_{i,i}(0^-). \tag{80}$$

Since the exact ground state of the Hubbard dimer is a singlet, let us consider first the antiferromagnetic Hartree-Fock solution ($m_+{=}0$ and $m_-{\neq}0$). In this case, the Hartree-Fock self-energy depends on the site and the interaction couples states with different k. This becomes

clear rewriting the Green-function matrix in the basis of the bonding ($k = 0$) and anti-bonding ($k = \pi$) creation/annihilation operators

$$G^{\sigma}(i\nu_n) = \frac{1}{2}\begin{pmatrix} i\nu_n - \big(\varepsilon_d - t - \mu + \frac{1}{2}\sum_i \Sigma_{i\sigma}(i\nu_n)\big) & \frac{1}{2}\sum_i (-1)^{i-1}\Sigma_{i\sigma}(i\nu_n) \\ \frac{1}{2}\sum_i (-1)^{i-1}\Sigma_{i\sigma}(i\nu_n) & i\nu_n - \big(\varepsilon_d + t - \mu + \frac{1}{2}\sum_i \Sigma_{i\sigma}(i\nu_n)\big) \end{pmatrix}^{-1}. \quad (81)$$

The diagonal terms of the matrix $\Sigma^{\sigma}_{k,k'}(i\nu_n)$ are thus identical

$$\Sigma^{\sigma}_{0,0}(i\nu_n) = \Sigma^{\sigma}_{\pi,\pi}(i\nu_n) = \frac{1}{2}\big(\Sigma^{\sigma}_{1,1}(i\nu_n) + \Sigma^{\sigma}_{2,2}(i\nu_n)\big). \quad (82)$$

The off-diagonal terms $\Sigma^{\sigma}_{0,\pi}(i\nu_n)$ and $\Sigma^{\sigma}_{\pi,0}(i\nu_n)$ are not zero, however. This tells us that, by introducing the antiferromagnetic HF correction, we lower the symmetry of the system. Let us now calculate explicitly the eigenstates for different fillings. It is sufficient to diagonalize $\hat{H}_1$, the Hamiltonian in the 1-electron sector; the many-electron states can be obtained by filling the one-electron states respecting the Pauli principle. The Hamiltonian $\hat{H}_1$ can be written as $\hat{H}_1 = \hat{H}'_1 + \varepsilon_d \hat{N} - \Delta_0$, and, in the antiferromagnetic case we then have

$$\hat{H}'_1 = \begin{pmatrix} U\big(\frac{1}{2}n - m_-\big) & -t & 0 & 0 \\ -t & U\big(\frac{1}{2}n + m_-\big) & 0 & 0 \\ 0 & 0 & U\big(\frac{1}{2}n + m_-\big) & -t \\ 0 & 0 & -t & U\big(\frac{1}{2}n - m_-\big) \end{pmatrix}. \quad (83)$$

This leads to the (normalized) states

$\lvert 1\rangle_l$	$E_l(1)$
$\lvert 1\rangle_3 = a_2\lvert 1, 1/2, \uparrow\rangle_1 - a_1\lvert 1, 1/2, \uparrow\rangle_2$	$\varepsilon_0(1) + \Delta_1(t,U)$
$\lvert 1\rangle_2 = a_1\lvert 1, 1/2, \downarrow\rangle_1 - a_2\lvert 1, 1/2, \downarrow\rangle_2$	$\varepsilon_0(1) + \Delta_1(t,U)$
$\lvert 1\rangle_1 = a_1\lvert 1, 1/2, \uparrow\rangle_1 + a_2\lvert 1, 1/2, \uparrow\rangle_2$	$\varepsilon_0(1) - \Delta_1(t,U)$
$\lvert 1\rangle_0 = a_2\lvert 1, 1/2, \downarrow\rangle_1 + a_1\lvert 1, 1/2, \downarrow\rangle_2$	$\varepsilon_0(1) - \Delta_1(t,U)$

where $\varepsilon_0(1) = \varepsilon_d + U\big(1/2 + 2m_-^2 - n^2/2\big)$ and $a_1^2 = \frac{1}{2}\left(1 + \frac{Um_-}{\Delta_1(t,U)}\right)$, while $\Delta_1(t,U) = \sqrt{(m_- U)^2 + t^2}$. At half filling, if we assume that only the ground doublet is occupied, solving the self-consistent equations (80) yields

$$m_- = 0 \quad \text{or} \quad m_- = \frac{1}{2}\sqrt{1 - \frac{4t^2}{U^2}}\,. \quad (84)$$

As a result, for the non-trivial solution ($m_- \neq 0$), the gap at half filling is $E_g^{\mathrm{HF}} = 2\Delta_1(t,U) = U$. In Fig. 6, Hartree-Fock and exact spectral function are compared for a specific parameter choice. Looking at the size of the gap only, one could naively infer that, for the case shown, Hartree-Fock is an excellent approximation, better than DMFT (see Fig. 3, top-right panel). This would

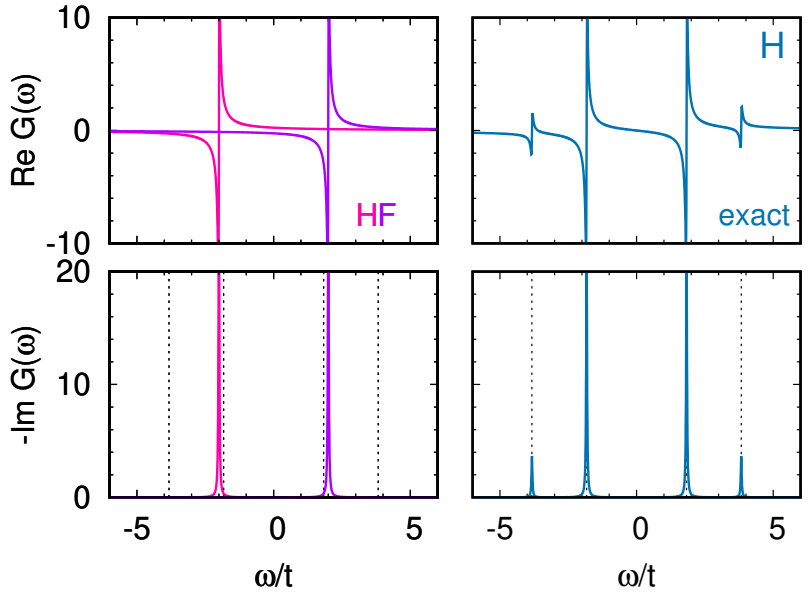

Fig. 6: *Local retarded Green function $G^\sigma(\omega)$ of the Hubbard dimer ($t = 1, U = 4$) at half filling and in the zero temperature limit. Left: Antiferromagnetic Hartree-Fock (HF) approximation; green and violet distinguish $G^\uparrow(\omega)$ and $G^\downarrow(\omega)$ at a given site. Right: Exact local Green function, for which $G^\uparrow(\omega) = G^\downarrow(\omega)$. Dashed lines: Poles of the exact local Green function.*

be, however, the wrong conclusion. Although, due to the small coordination number, in this specific case, DMFT indeed sizably underestimates the gap, it nevertheless captures the essential nature of the ground state. Instead, while HF, in this specific case,[6] gives an almost exact gap, it does it via a qualitatively incorrect description (antiferromagnetic instead of singlet ground state). Increasing the coordination number, DMFT approaches the exact solution both in the paramagnetic and magnetic phase, while HF does not. Let us analyze in more detail the differences between the HF approximation and the exact solution of the Hubbard dimer. The HF Hamiltonian for two electrons is given by $\hat{H}_2 = \hat{H}_2' + \varepsilon_d \hat{N} - \Delta_0$, and

$$\hat{H}_2' = \begin{pmatrix} U & 0 & 0 & -2Um_- & 0 & 0 \\ 0 & U(1-2m_+) & 0 & 0 & 0 & 0 \\ 0 & 0 & U(1+2m_+) & 0 & 0 & 0 \\ -2Um_- & 0 & 0 & U & -\sqrt{2}t & -\sqrt{2}t \\ 0 & 0 & 0 & -\sqrt{2}t & U & 0 \\ 0 & 0 & 0 & -\sqrt{2}t & 0 & U \end{pmatrix}. \quad (85)$$

[6] In real materials the Hartree-Fock approximation often overestimates the size of the gap, however.

For m_+=0 and $m_- \neq 0$ (antiferromagnetic solution) the eigenvalues and eigenvectors are

$\|2\rangle_l$	$E_l(2)$
$\|2\rangle_5 = \frac{1}{\sqrt{2}}\Big(\|2,0,0\rangle_0 + a_2\|2,1,0\rangle - \frac{a_1}{\sqrt{2}}\big(\|2,0,0\rangle_1 + \|2,0,0\rangle_2\big)\Big)$	$\varepsilon_0(2) + 2\Delta_1(t,U)$
$\|2\rangle_4 = \frac{1}{\sqrt{2}}\big(\|2,0,0\rangle_1 - \|2,0,0\rangle_2\big)$	$\varepsilon_0(2)$
$\|2\rangle_3 = \|2,1,1\rangle$	$\varepsilon_0(2)$
$\|2\rangle_2 = \|2,1,-1\rangle$	$\varepsilon_0(2)$
$\|2\rangle_1 = a_1\|2,1,0\rangle + a_2\frac{1}{\sqrt{2}}\big(\|2,0,0\rangle_1 + \|2,0,0\rangle_2\big)$	$\varepsilon_0(2)$
$\|2\rangle_0 = \frac{1}{\sqrt{2}}\Big(\|2,0,0\rangle_0 - a_2\|2,1,0\rangle + \frac{a_1}{\sqrt{2}}\big(\|2,0,0\rangle_1 + \|2,0,0\rangle_2\big)\Big)$	$\varepsilon_0(2) - 2\Delta_1(t,U)$

where $\varepsilon_0(2)$=$2\varepsilon_d + U\big(1+2m_-^2 - n^2/2\big)$, and $a_1^2 = t^2/\Delta_1^2(t,U)$. The antiferromagnetic Hartree-Fock ground state has an overlap with the correct ground state, however incorrectly mixes triplet and singlet states, thus breaking the rotational symmetry of the model. For this reason, its energy, in the large U limit, is $2\varepsilon_d - 2t^2/U$ and not $2\varepsilon_d - 4t^2/U$ as in the exact case.
For the ferromagnetic solution of the Hartree-Fock equations (m_-=0 and $m_+ \neq 0$) the eigenvalues and eigenvectors are instead

$\|2\rangle_l$	$E_l(2)$
$\|2\rangle_5 = \|2,1,-1\rangle$	$\varepsilon_0^+(2) + 2Um_+$
$\|2\rangle_4 = \frac{1}{\sqrt{2}}\Big(\|2,0,0\rangle_0 - \frac{1}{\sqrt{2}}\big(\|2,0,0\rangle_1 + \|2,0,0\rangle_2\big)\Big)$	$\varepsilon_0^+(2) + 2t$
$\|2\rangle_3 = \frac{1}{\sqrt{2}}\big(\|2,0,0\rangle_1 - \|2,0,0\rangle_2\big)$	$\varepsilon_0^+(2)$
$\|2\rangle_2 = \|2,1,\ \ 0\rangle$	$\varepsilon_0^+(2)$
$\|2\rangle_1 = \frac{1}{\sqrt{2}}\Big(\|2,0,0\rangle_0 + \frac{1}{\sqrt{2}}\big(\|2,0,0\rangle_1 + \|2,0,0\rangle_2\big)\Big)$	$\varepsilon_0^+(2) - 2t$
$\|2\rangle_0 = \|2,1,\ \ 1\rangle$	$\varepsilon_0^+(2) - 2Um_+$

where $\varepsilon_0^+(2)$=$2\varepsilon_d + U(1 + 2m_+^2 - n^2/2)$. The ferromagnetic Hartree-Fock correction thus yields an incorrect sequence of levels; the ground state for large U/t, indicated as $|2\rangle_0$ in the table, has no overlap with the exact ground state of the Hubbard dimer. It is, instead, one of the states of the first excited triplet. An important observation is that, despite the errors, the energy difference between ferro- and antiferro-magnetic ground state is

$$E_{\rm F} - E_{\rm AF} \sim \frac{2t^2}{U}, \tag{86}$$

which is indeed the correct value in the small t/U limit. It does not correspond, however, to the actual singlet-triplet excitation energy, $\Gamma \sim 4t^2/U$.

We can now directly compare the **Hartree-Fock** and the **dynamical mean-field approximation** for the two-site Hubbard model. Both approaches are based on the solution of self-consistent mean-field-type equations, and therefore they are both mean-field methods. In Hartree-Fock the self-energy is frequency-independent (static), while in DMFT depends on the frequency (dynamical). In Hartree-Fock the self-energy can be site-dependent, as we have seen in the antiferromagnetic case. In DMFT, allowing for a site-dependent self-energy leads to cluster or cluster-like extensions of the method. If the same unit cell is used in DMFT and Hartree-Fock, we can identify another relation between the two methods. In the infinite-frequency limit, the DMFT self-energy equals the Hartree-Fock self-energy. This can be shown analytically in a simple way. For the case of the two-site Hubbard model, the expansion of the local lattice Green function at high frequency in the local-self-energy approximation is

$$G^\sigma_{i,i}(i\nu_n) = \frac{1}{i\nu_n} - \frac{\big(\mu - \varepsilon_d - \Sigma^\sigma_l(\infty)\big)}{(i\nu_n)^2} + \mathcal{O}\bigg(\frac{1}{(i\nu_n)^3}\bigg). \tag{87}$$

Instead, the expansion of the impurity Green-function can be written as

$$\begin{aligned} G^\sigma_{d,d}(i\nu_n) &= \int_0^\beta d\tau\, e^{i\nu_n\tau} G^\sigma_{d,d}(\tau) \\ &= \frac{1}{i\nu_n}\int_0^\beta d\tau \frac{de^{i\nu_n\tau}}{d\tau} G^\sigma_{d,d}(\tau) = \frac{1}{i\nu_n}\bigg(- G^\sigma_{d,d}(\beta^-) - G^\sigma_{d,d}(0^+) - \int_0^\beta d\tau\, e^{i\nu_n\tau}\frac{dG^\sigma_{d,d}(\tau)}{d\tau}\bigg) \\ &= \frac{1}{i\nu_n} + \frac{1}{(i\nu_n)^2}\bigg(\frac{dG^\sigma_{d,d}(\tau)}{d\tau}\bigg|_{\beta^-} + \frac{dG^\sigma_{d,d}(\tau)}{d\tau}\bigg|_{0^+} + \int_0^\beta d\tau\, e^{i\nu_n\tau}\frac{d^2G^\sigma_{d,d}(\tau)}{d\tau^2}\bigg) \\ &= \frac{1}{i\nu_n} + \frac{\frac{dG^\sigma_{d,d}(\tau)}{d\tau}\Big|_{\beta^-} + \frac{dG^\sigma_{d,d}(\tau)}{d\tau}\Big|_{0^+}}{(i\nu_n)^2} + \mathcal{O}\bigg(\frac{1}{(i\nu_n)^3}\bigg) \end{aligned} \tag{88}$$

where

$$\frac{dG^\sigma_{d,d}(\tau)}{d\tau}\bigg|_{\beta^-} + \frac{dG^\sigma_{d,d}(\tau)}{d\tau}\bigg|_{0^+} = -\bigg\langle\Big\{\big[\hat{H}_A - \mu\hat{N},\, c_{d\sigma}\big],\, c^\dagger_{d\sigma}\Big\}\bigg\rangle = -\mu + \varepsilon_d + U\langle\hat{n}_{-\sigma}\rangle. \tag{89}$$

From this result we can conclude that, assuming self-consistency has been reached,

$$\Sigma^\sigma_l(\infty) = U\langle\hat{n}_{-\sigma}\rangle. \tag{90}$$

This is exactly the Hartree-Fock expression of the self-energy that we found earlier, and indeed equals the **infinite-frequency limit** of the DMFT self-energy we previously calculated; however, the occupations $\langle\hat{n}_{-\sigma}\rangle$ in DMFT and Hartree-Fock calculations are typically not the same. In the case of the dimer, DMFT yields $\langle\hat{n}_{-\sigma}\rangle$=1/2; this would correspond in Hartree-Fock to a (trivial) solution in which the self-energy merely shifts all the energy levels by the same amount, and has therefore no relevant effects. These conclusions also apply to the LDA+U method, which is based on the Hartree-Fock treatment of the local Coulomb interaction. A more detailed discussion of differences and relation between the LDA+U and LDA+DMFT method can be found in my chapter in Ref. [14].

2.5 DMFT for the one-band Hubbard model

The Hubbard Hamiltonian (8) is in principle the simplest model for the description of the Mott metal-insulator transition. In the tight-binding approximation it becomes

$$\hat{H} = \varepsilon_d \sum_{\sigma i} \hat{n}_{i\sigma} - t \sum_{\sigma\langle ii'\rangle} c^\dagger_{i\sigma} c_{i'\sigma} + U \sum_i \hat{n}_{i\uparrow}\hat{n}_{i\downarrow}, \tag{91}$$

where $\langle ii'\rangle$ is a sum over first neighbors. As discussed in the introduction, for $U{=}0$, at half-filling, this Hamiltonian describes a metallic band. For $t{=}0$ it describes an insulating collection of disconnected atoms. Somewhere in between, at a critical value of t/U, a metal to insulator transition must occur. In this section we will discuss the DMFT solution of (91) and the picture of the metal-insulator transition emerging from it. The first step consists in mapping the original many-body Hamiltonian into an effective quantum-impurity model, such as the Anderson Hamiltonian

$$\hat{H}^A = \underbrace{\sum_{\boldsymbol{k}\sigma} \varepsilon^s_{\boldsymbol{k}} \hat{n}_{\boldsymbol{k}\sigma}}_{\hat{H}_{\rm bath}} + \underbrace{\sum_{\boldsymbol{k}\sigma} \left(V^s_{\boldsymbol{k}} c^\dagger_{\boldsymbol{k}\sigma} c_{d\sigma} + \text{h.c.} \right)}_{\hat{H}_{\rm hyb}} + \underbrace{\varepsilon_d \sum_\sigma \hat{n}_{d\sigma} + U \hat{n}_{d\uparrow}\hat{n}_{d\downarrow}}_{\hat{H}_{\rm imp}}. \tag{92}$$

In this model the on-site Coulomb repulsion U appears only in the impurity Hamiltonian, $\hat{H}_{\rm imp}$, while the terms $\hat{H}_{\rm bath}$ and $\hat{H}_{\rm hyb}$, describe, respectively, the bath and the bath-impurity hybridization. In the next step, the quantum-impurity model is solved. Differently from the case of the Anderson molecule, this cannot be done analytically. It requires non-perturbative numerical methods, such as exact diagonalization, the numerical renormalization group, density-matrix renormalization group or QMC. Here we describe the DMFT self-consistency loop for a QMC quantum-impurity solver. Solving the quantum-impurity model yields the impurity Green function $G^\sigma_{d,d}(i\nu_n)$. From the impurity Dyson equation we can calculate the impurity self-energy

$$\Sigma^\sigma_A(i\nu_n) = \left(G^{0\sigma}_{d,d}(i\nu_n)\right)^{-1} - \left(G^\sigma_{d,d}(i\nu_n)\right)^{-1}. \tag{93}$$

Next, we adopt the local self-energy approximation, i.e., we assume that the self-energy of the Hubbard model equals the impurity self-energy. Then, the local Green function is given by

$$G^\sigma_{i_c,i_c}(i\nu_n) = \frac{1}{N_{\boldsymbol{k}}} \sum_{\boldsymbol{k}} \frac{1}{i\nu_n + \mu - \varepsilon_{\boldsymbol{k}} - \Sigma^\sigma_A(i\nu_n)}, \tag{94}$$

where $N_{\boldsymbol{k}}$ is the number of $\boldsymbol{k}$ points. The local Dyson equation is used once more, this time to calculate the bath Green function $\mathcal{G}^\sigma(i\nu_n)$, which in turn defines a new quantum-impurity model. This procedure is repeated until self-consistency is reached, i.e., the number of electrons is correct and the self-energy does not change anymore (within a given numerical accuracy). In this situation we have

$$G^\sigma_{i_c,i_c}(i\nu_n) \sim G^\sigma_{d,d}(i\nu_n). \tag{95}$$

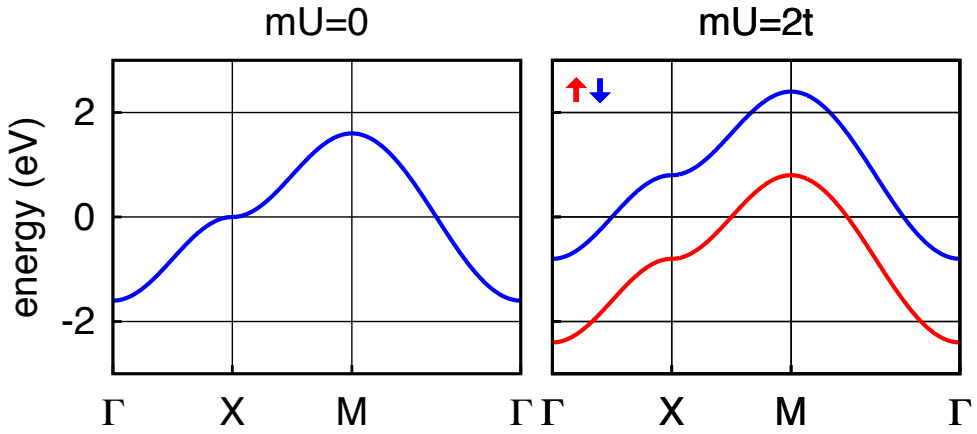

Fig. 7: *The metal-insulator transition in ferromagnetic Hartree-Fock. The calculation is for a square lattice tight-binding model with dispersion* $\varepsilon_{\boldsymbol{k}} = -2t(\cos k_x + \cos k_y)$.

It is important to underline that self-consistency is key to the success of DMFT in describing the metal-to-insulator transition. This can, perhaps, be best understood looking once more at the effects of self-consistency in a simpler approach, the static mean-field Hartree-Fock method.[7] If we chose the same primitive cell as in DMFT, the Hartree-Fock self-energy matrix is

$$\Sigma^{\sigma}_{i,i'}(i\nu_n) = U\left(\frac{n}{2} - \sigma m\right)\delta_{i,i'}, \tag{96}$$

where $\sigma = +1$ for spin up and $\sigma = -1$ for spin down and $m{=}m_+{=}(n_\uparrow - n_\downarrow)/2$, with $n_\sigma{=}n_{i\sigma}$. The approximation is then identical to replacing the Hubbard Hamiltonian with

$$\hat{H}_{\rm HF} = \sum_{\boldsymbol{k}\sigma}\left[\varepsilon_{\boldsymbol{k}} + U\left(\frac{1}{2} - \sigma m\right)\right]\hat{n}_{\boldsymbol{k}\sigma}. \tag{97}$$

This shows that $h_{\rm eff}{=}2Um$ plays the role of an effective magnetic field (Weiss field). The self-consistency criterion is

$$\bar{n}_\sigma = \bar{n}_{i\sigma} = \langle\hat{n}_{i\sigma}\rangle_{\rm HF}\,, \tag{98}$$

where the expectation value $\langle\hat{n}_{i\sigma}\rangle_{\rm HF}$ is calculated using the Hamiltonian $\hat{H}_{\rm HF}$, which in turn depends on $\bar{n}_\sigma$ via m. This gives the self-consistency equation

$$m = \frac{1}{2}\frac{1}{N_{\boldsymbol{k}}}\sum_{\boldsymbol{k}\sigma}\frac{\sigma e^{-\beta(\varepsilon_{\boldsymbol{k}}+U(\frac{1}{2}-\sigma m)-\mu)}}{1+e^{-\beta(\varepsilon_{\boldsymbol{k}}+U(\frac{1}{2}-\sigma m)-\mu)}}\,. \tag{99}$$

If we set $m{=}0$ the equation is satisfied; for such a trivial solution the static mean-field correction in Eq. (97) merely redefines the chemical potential and has therefore no effect. For sufficiently large U, however, a non-trivial solution ($m \neq 0$) can be found. If $m \neq 0$ the spin up and spin down bands split, and eventually a gap can open. This is shown in Fig. 7. The static mean-field correction in Eq. (97) equals the contribution of the Hartree diagram to the self-energy, $\Sigma^{\sigma}_{\rm H}(i\nu_n){=}U\bar{n}_{-\sigma}$. In many-body perturbation theory, however, $\bar{n}_\sigma{=}1/2$, i.e., $m{=}0$.

[7] Keeping in mind that many self-consistent solutions obtained with the Hartree-Fock method are spurious.

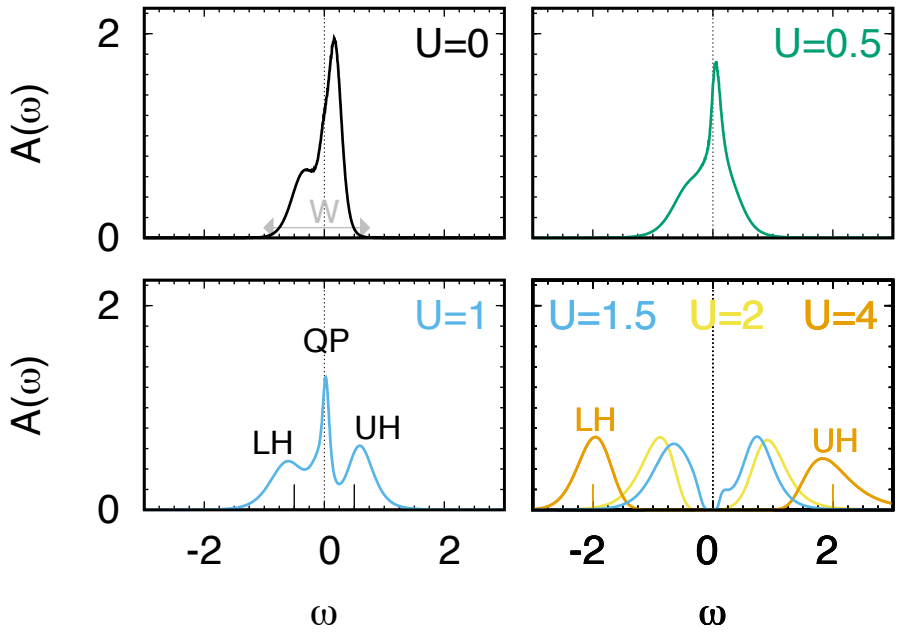

Fig. 8: *$VOMoO_4$: LDA+DMFT spectral function at finite temperature for $0 \leq U \leq 4$. Energies are in eV and spectral functions in states/spin/eV. The calculations have been done using a continuous-time hybridization-expansion QMC solver [13]. A detailed LDA+DMFT study of the electronic and magnetic properties of $VOMoO_4$ can be found in Ref. [15].*

In the self-consistent static mean-field approximation, instead, m can differ from zero, and a phenomenon not described by the mere Hartree diagram can be captured, ferromagnetism in a correlated metal. If mU is larger than the bandwidth, the system can even become an insulator. In DMFT the role of the Weiss mean field is played by the bath Green function $\mathcal{G}^{\sigma}_{i,i}(i\nu_n)$. The emerging picture of the Mott transition is described in Fig. 8 for a representative single-band material. In the U=0 limit, the spectral function $A_0(\omega)$ is metallic at half filling (top left panel). For finite U, if we set $\Sigma^{\sigma}_A(\omega)$=0 as initial guess, the DMFT self-consistency loop starts with $A(\omega)$=$A_0(\omega)$. For small U/t, the *converged* spectral function $A(\omega)$ is still similar to $A_0(\omega)$. This can be seen comparing the U=0.5 and U=0 panels in Fig. 8. Further increasing U/t, sizable spectral weight is transferred from the zero-energy quasi-particle peak to the lower (LH) and upper (UH) Hubbard bands, centered at $\omega \sim \pm U/2$. This can be observed in the $U = 1$ panel of Fig. 8. The system is still metallic, but with strongly renormalized masses and short lifetimes, reflected in the narrow quasi-particle (QP) peak. Finally, for U larger than a critical value ($U \geq 1.5$ in the figure) a gap opens and the system becomes a Mott insulator. When this happens the self-energy diverges at low frequency, where

$$\Sigma^{\sigma}_A(\omega + i0^+) \sim \frac{U}{2} + \frac{U^2}{4}\frac{a(t,U)}{\omega + i0^+}. \tag{100}$$

In the large U/t limit the gap increases linearly with the Coulomb repulsion, i.e., $E_g(1) \sim U-W$, where W is the bandwidth.

2.6 DMFT for multi-orbital models

The multi-orbital Hubbard-like Hamiltonian has the form

$$\hat{H} = \hat{H}_0 + \hat{H}_U \tag{101}$$

$$\hat{H}_0 = -\sum_{ii'}\sum_{\sigma\sigma'}\sum_{mm'} t^{i,i'}_{m\sigma,m'\sigma'}\, c^\dagger_{im\sigma} c_{i'm'\sigma'} \tag{102}$$

$$\hat{H}_U = \frac{1}{2}\sum_{i}\sum_{\sigma\sigma'}\sum_{mm'}\sum_{pp'} U_{mpm'p'}\, c^\dagger_{im\sigma} c^\dagger_{ip\sigma'} c_{ip'\sigma'} c_{im'\sigma}, \tag{103}$$

where m, m' and p, p' are different orbitals and the Coulomb tensor is local. The DMFT approach can be extended to solve models of this form, mapping them to multi-orbital quantum-impurity models. The main changes with respect to the formalism introduced in the previous section are then the following

$$\varepsilon_{\boldsymbol{k}} \to (H_{\boldsymbol{k}})_{m\sigma,m'\sigma'} \qquad (i\nu_n{+}\mu) \to (i\nu_n{+}\mu)\,\hat{1}_{m\sigma,m'\sigma'}$$

$$t^{i,i'} \to t^{i,i'}_{m\sigma,m'\sigma'} \qquad \varepsilon_d \to \varepsilon^{i,i'}_{m\sigma,m'\sigma'} = -t^{i,i}_{m\sigma,m'\sigma'}$$

where $\hat{1}$ is the identity matrix. As a consequence, the local Green function, the bath Green function, the hybridization function, and the self-energy also become matrices

$$\mathcal{G}^\sigma(i\nu_n) \to \mathcal{G}^{\sigma,\sigma'}_{m,m'}(i\nu_n) \qquad G^\sigma(i\nu_n) \to G^{\sigma,\sigma'}_{m,m'}(i\nu_n) \qquad \Sigma^\sigma(i\nu_n) \to \Sigma^{\sigma,\sigma'}_{m,m'}(i\nu_n).$$

The corresponding generalization of the self-consistency loop is shown schematically in Fig. 9. Although the extension of DMFT to Hubbard models with many orbitals might appear straightforward, in practice it is not. The bottleneck is the solution of the generalized multi-orbital quantum-impurity problem. The most flexible solvers available so far are all based on QMC. Despite being flexible, QMC-based approaches have limitations. These can be classified in two types. First, with increasing the number of degrees of freedom, calculations become very quickly computationally too expensive—how quickly depends on the specific QMC algorithm used and the actual implementation. Thus, typically, going beyond a limited number of orbitals and reaching the zero-temperature limit is unfeasible in practice. The second type of limitation is more severe. Increasing the number of degrees of freedom leads, eventually, to the infamous sign problem; when this happens, QMC calculations cannot be performed at all. In order to deal with limitations of the first type, it is crucial to restrict QMC calculations to the essential degrees of freedom; furthermore, we should exploit symmetries, develop fast algorithms and use the power of massively-parallel supercomputers to reduce the actual computational time. For the second type of problems not a lot can be done; nevertheless, it has been shown that a severe sign problem might appear earlier with some basis choices than with others [13]. Although eventually we cannot escape it, this suggests that the model set up can be used as a tool to expand the moderate sign-problem zone. For what concerns symmetries, in the paramagnetic case and in absence of spin-orbit interaction or external fields, an obvious symmetry to exploit

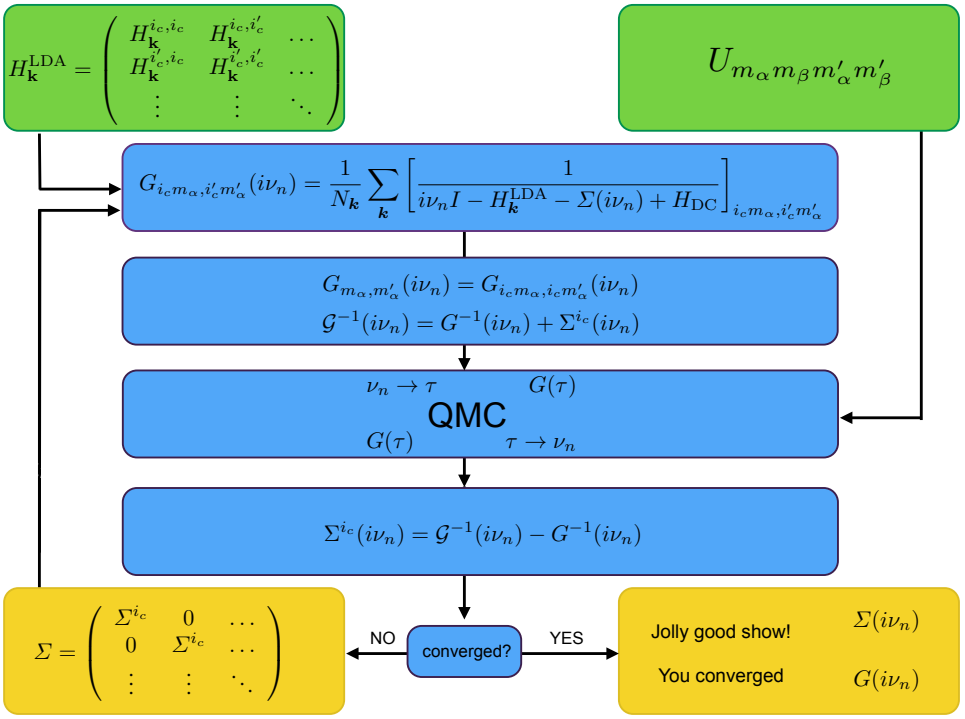

Fig. 9: *LDA+DMFT self-consistency loop. The one-electron Hamiltonian is built in the basis of Bloch states obtained from localized Wannier functions, for example in the local-density approximation (LDA); this gives $H^{\mathrm{LDA}}_{\boldsymbol{k}}$. The set $\{i_c\}$ labels the equivalent correlated sites inside the unit cell. The local Green-function matrix is at first calculated using an initial guess for the self-energy matrix. The bath Green-function matrix is then obtained via the Dyson equation and used to construct an effective quantum-impurity model. The latter is solved via a quantum-impurity solver, here quantum Monte Carlo (QMC). This yields the impurity Green-function matrix. Through the Dyson equation the self-energy is then obtained, and the procedure is repeated until self-consistency is reached.*

is the rotational invariance of spins, from which follows

$$A^{\sigma,\sigma'}_{m,m'}(i\nu_n) = \delta_{\sigma,\sigma'}\, A_{m,m'}(i\nu_n), \tag{104}$$

where $A = \mathcal{G}, G, \Sigma$. In addition, if we use a basis of real functions, the local Green-function matrices are real and symmetric in imaginary time τ, hence

$$A^{\sigma,\sigma'}_{m,m'}(i\nu_n) = \delta_{\sigma,\sigma'}\, A_{m,m'}(i\nu_n) = \delta_{\sigma,\sigma'}\, A_{m',m}(i\nu_n). \tag{105}$$

Finally, often the unit cell contains several equivalent correlated sites, indicated as $\{i_c\}$ in Fig. 9. In order to avoid expensive cluster calculations, we can use space-group symmetries to construct the matrices $\mathcal{G}, G, \Sigma$ at a given site i'_c from the corresponding matrices at an equivalent site, e.g., $i_c = 1$. Space-group symmetries also tell us if some matrix elements are zero. For example, for a model with only t_{2g} (or only e_g) states, in cubic symmetry, in the paramagnetic case and in absence of spin-orbit interaction or external fields, we have

$$A^{\sigma,\sigma'}_{m,m'}(i\nu_n) = \delta_{\sigma,\sigma'}\, A_{m,m}(i\nu_n)\, \delta_{m,m'}. \tag{106}$$

3 Building materials-specific many-body models

3.1 Model construction

How do we build realistic Hubbard-like models for correlated materials? The state-of-the art approach relies on constructing, for a given system, *materials-specific* Kohn-Sham Wannier functions $\varphi^{\rm KS}_{im\sigma}(\boldsymbol{r})$. These can be obtained via electronic structure calculations based on density-functional theory [8–10], e.g., in the LDA approximation.[8] After we constructed the complete one-electron basis, the first steps in model-building are those described in the introduction. We recall here the essential points and then discuss the next stage. The many-body Hamiltonian can be expressed as $\hat{H} = \hat{H}_0 + \hat{H}_U - \hat{H}_{\rm DC}$, with $\hat{H}_0 = \hat{H}^{\rm LDA}$ and

$$\hat{H}_0 = -\sum_{ii'}\sum_{\sigma\sigma'}\sum_{mm'} t^{i,i'}_{m\sigma,m'\sigma'} c^\dagger_{im\sigma} c_{i'm'\sigma'}, \tag{107}$$

$$\hat{H}_U = \frac{1}{2}\sum_{ii'jj'}\sum_{\sigma\sigma'}\sum_{mm'pp'} U^{iji'j'}_{mp\,m'p'} c^\dagger_{im\sigma} c^\dagger_{jp\sigma'} c_{j'p'\sigma'} c_{i'm'\sigma}. \tag{108}$$

The hopping integrals in $\hat{H}_0$ are calculated replacing the electron-nuclei interaction, $v_{\rm en}(\boldsymbol{r})$, with the self-consistent DFT reference potential, $v_{\rm R}(\boldsymbol{r}) = v_{\rm en}(\boldsymbol{r}) + v_{\rm H}(\boldsymbol{r}) + v_{\rm xc}(\boldsymbol{r})$, defined in Eq. (5). The latter includes the long-range Hartree term, $v_{\rm H}(\boldsymbol{r})$, and the exchange-correlation contribution, $v_{\rm xc}(\boldsymbol{r})$; to avoid including the *effects* of these terms twice, we thus introduce the double-counting correction, $\hat{H}_{\rm DC}$, so that

$$\hat{H}_U \to \Delta\hat{H}_U = \hat{H}_U - \hat{H}_{\rm DC}.$$

Unfortunately we do not know which important correlation effects are included in $\hat{H}_0$ via $v_{\rm R}(\boldsymbol{r})$, and therefore the exact expression of $\Delta\hat{H}_U$ is also unknown. The remarkable successes of the LDA suggest, however, that in many materials the LDA is overall a good approximation, and therefore, in those systems at least, the term $\Delta\hat{H}_U$ can be completely neglected. What about strongly-correlated materials? Even in correlated systems, most likely, the LDA works rather well for the delocalized electrons or in describing the average or the long-range Coulomb effects. Thus one can think of separating the electrons into two categories: *uncorrelated* (or light) and *correlated* (or heavy); only for the latter we do take the correction $\Delta\hat{H}_U$ into account explicitly, assuming furthermore that $\Delta\hat{H}_U$ is local or almost local [8], since we know that it is the local term which is responsible for most non-trivial many-body effects. Typically, correlated electrons are those that partially retain their atomic character, e.g., those that originate from localized d and f shells; for convenience, here we assume that in a given system they stem from a single atomic shell l (e.g., d for transition-metal oxides or f for heavy-fermion systems) and label their states with the atomic quantum numbers l and $m = -l, \ldots, l$ of that shell. Thus

$$U^{iji'j'}_{mp\,m'p'} \sim \begin{cases} U^l_{mp\,m'p'} & iji'j' = iiii \quad \wedge \quad mp, m'p' \in l \\ 0 & iji'j' \neq iiii \quad \vee \quad mp, m'p' \notin l. \end{cases}$$

[8] Using GGA or similar functionals in place of LDA yields minor differences in the many-body Hamiltonian; on the other hand, using LDA+U or similar approximations yields Hartree-Fock-like effects that would have to be subtracted via the double-counting correction.

Within this approximation $\Delta\hat{H}_U$ is replaced by $\Delta\hat{H}^l_U = \hat{H}^l_U - \hat{H}^l_{\rm DC}$, where $\hat{H}^l_{\rm DC}$ is, e.g., given by the static mean-field contribution of $\hat{H}^l_U$. There is a drawback in this procedure, however. By splitting electrons into light and heavy, we implicitly assume that the main effect of the latter is the renormalization or *screening* of parameters for the former, in particular of the Coulomb interaction. The computation of screening effects remains, unfortunately, a challenge. The calculation of exact screening would require the solution of the original many-body problem, taking all degrees of freedom into account, an impossible task. Commonly-used approximate schemes are the constrained LDA approximation (cLDA) and the constrained random-phase approximation (RPA) [8–10]. Both methods give reasonable estimates of screened Coulomb parameters for DMFT calculations. Typically cRPA calculations include more screening channels and are performed for less localized bases than cLDA calculations; thus cRPA parameters turn out to be often smaller than cLDA ones. To some extent, the difference can be taken as an estimate of the error bar.

After we have selected the electrons for which we think it is necessary to include explicitly the Hubbard correction, in order to build the final Hamiltonian for DMFT calculations, it is often convenient to integrate out or *downfold*, in part or completely, the weakly correlated states. There are different degrees of downfolding. The two opposite extreme limits are (i) *no downfolding*, i.e., keeping explicitly in the Hamiltonian all weakly-correlated states (ii) *massive downfolding*, i.e., downfold all weakly correlated states. If we perform massive downfolding, e.g., downfold to the d (or e_g or t_{2g}) bands at the Fermi level, the Hamiltonian relevant for DMFT takes a simpler form. The LDA part is limited to the selected orbitals or bands, which, in the ideal case, are decoupled from the rest

$$\hat{H}^{\rm LDA} = -\sum_{ii'}\sum_{\sigma\sigma'}\sum_{m_\alpha m'_\alpha} t^{i,i'}_{m_\alpha\sigma,m'_\alpha\sigma'}\, c^\dagger_{im_\alpha\sigma}\, c_{i'm'_\alpha\sigma'}. \tag{109}$$

The local *screened* Coulomb interaction for this set of orbitals is the on-site tensor

$$\hat{H}^l_U = \frac{1}{2}\sum_{i}\sum_{\sigma\sigma'}\sum_{m_\alpha m'_\alpha}\sum_{m_\beta m'_\beta} U_{m_\alpha m_\beta m'_\alpha m'_\beta}\, c^\dagger_{im_\alpha\sigma} c^\dagger_{im_\beta\sigma'} c_{im'_\beta\sigma'} c_{im'_\alpha\sigma}. \tag{110}$$

It is important to point out that the level of downfolding does not modify the hardness of the quantum-impurity problem. If, for example, in studying a transition-metal oxide, we plan to treat only $3d$ bands as correlated, it does not matter if we perform calculations with a Hamiltonian containing also, e.g., O p states, or we rather downfold all states but the $3d$ and work with a set of Wannier basis spanning the $3d$-like bands only. The number of correlated orbitals in the quantum-impurity problem is the same.[9]

One advantage of massive downfolding is that the double-counting correction typically becomes a shift of the chemical potential, and it is therefore not necessary to calculate it explicitly. A second important advantage is that the interpretation of the final results is simpler. Instead, a disadvantage is that the basis functions are less localized, and therefore the approximation of the Coulomb interaction to a local operator might be less justified, and in some cases it might be

[9] The choice might influence how severe the QMC sign problem is, however.

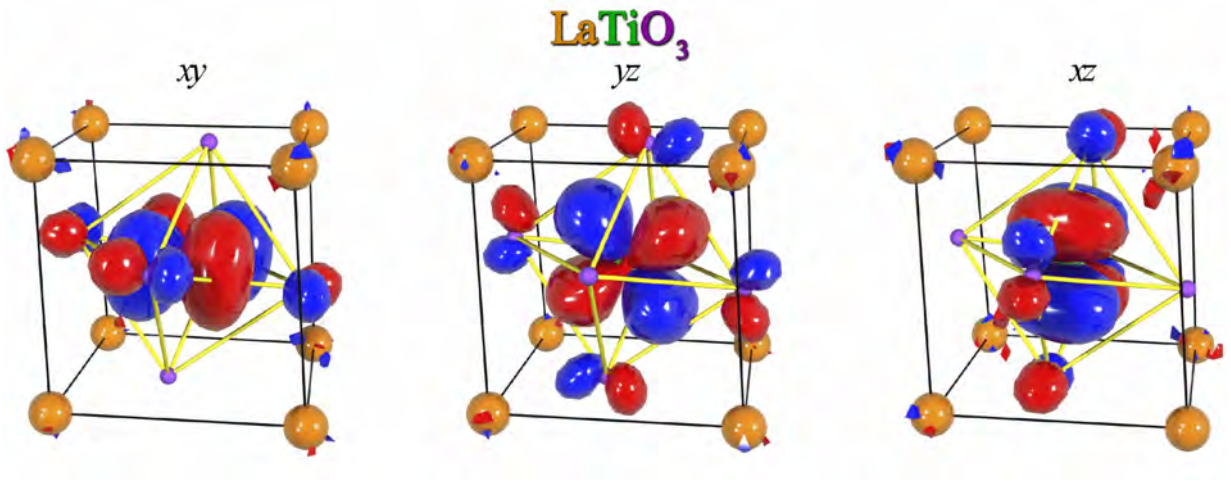

Fig. 10: *NMTO Wannier-like orbitals for t_{2g} states in $LaTiO_3$ obtained via massive downfolding to the t_{2g} bands. The t_{2g}-like orbitals have O p tails at the neighboring O sites reflecting the distortions of the lattice. The figure has been taken from Ref. [16].*

necessary to include non-local Coulomb terms. The effect of downfolding on the localization of Wannier functions is illustrated for example in Fig. 10. Finally, another disadvantage of massive downfolding is that the energy window in which the model is valid is more narrow.

Considering all advantages and disadvantages, what is then the best way of performing DMFT calculations? There is no universal answer to this question; it depends on the problem we are trying to solve and the system we are studying. Independently of the degree of downfolding we choose, it is important to point out that a clear advantage of Wannier functions in general is that they carry information about the lattice, bonding, chemistry and distortions. This can be seen once more in Fig. 10, where orbitals are tilted and deformed by the actual structure and chemistry of the compound. Indeed, one might naively think of using a "universal" basis, for example atomic functions, the same for all systems, and thus calculating the hopping integrals using simply the electron-nuclei interaction $v_{en}(\boldsymbol{r})$. Besides the complications arising from the lack of orthogonality, such a basis has no built-in materials-specific information, except lattice positions. It is therefore a worse starting point to describe the electronic structure, even in the absence of correlations; larger basis sets are required to reach the same accuracy. From the point of view of LDA+DMFT, an advantage of a universal basis would be that it is free from double-counting corrections; on the other hand, however, exactly because we do not use the LDA potential and LDA orbitals to calculate the hopping integrals, we also cannot count on the successes of LDA in the description of average and long-range Coulomb effects. For these reasons *ab-initio* Wannier functions remain so far the basis of choice. They can be built via the Nth-Order Muffin-Tin Orbital (NMTO) method [16], the maximal-localization scheme [17], or projectors. Fig. 10 shows examples of NMTO-based Wannier functions.

3.2 Localization of the basis and range of the Coulomb interaction

No matter what construction procedure is used, a common characteristic of *ab-initio* Wannier functions is that they are site-centered and localized.[10] A question naturally arises: How crucial is it to use localized functions as one-electron basis? This is an important point, since we have seen that strong-correlation effects arise in systems in which the on-site Coulomb interaction is much larger than longer-range terms. Let us consider therefore two opposite extreme limits. The first is the case in which the basis functions are independent of the lattice position (i.e., they are totally delocalized). For such a basis choice the Coulomb interaction parameters would be the same for every couple of lattice sites, no matter how distant. Thus a Hubbard-like model would be hard to justify. In the second extreme case, we adopt a hypothetical basis so localized that $\psi_{im\sigma}(\boldsymbol{r})\overline{\psi_{i'm'\sigma'}}(\boldsymbol{r}) \sim \delta_{i,i'}\delta(\boldsymbol{r}-\boldsymbol{T}_i)$. Even for such a basis choice, the unscreened Coulomb interaction is *not* local. It is given by

$$U^{iji'j'}_{mp\,m'p'} \propto \frac{\delta_{i,i'}\delta_{j,j'}}{|\boldsymbol{T}_i-\boldsymbol{T}_j|}\,, \tag{111}$$

hence it decays slowly with distance, although the (divergent) on-site term dominates. More generally, we can conclude that by increasing the localization of the basis we enhance the importance of the on-site Coulomb repulsion with respect to long-range terms; this better justifies Hubbard-like models—although we have to remember that most of the long-range part of the Coulomb interaction is in any case subtracted via the double-counting correction $\hat{H}_{\rm DC}$. The extreme case of the $\delta(\boldsymbol{r}-\boldsymbol{T}_i)$ functions also illustrates, however, how far we can go. A major problem with the extremely localized basis discussed above is that it would make it impossible to properly describe bonding, since the hopping integrals would be zero. Although such a basis is, of course, never used to build many-body models, there is a tempting approximation that has similar flaws. If one uses DFT-based electronic-structure techniques that tile the space in interstitial and *non*-overlapping atomic spheres (e.g., the LAPW method), it is tempting to use as basis for correlated electrons the atomic functions *defined inside the atomic spheres*. These functions are, by construction, much more localized than Wannier orbitals (even when no downfolding is performed in the Wannier construction). However, they *do not form a complete basis set* in the space of square-integrable functions. This is obvious because such a basis does not even span the LDA bands; to reproduce the bands we need, in addition, functions defined in the interstitial region. This is illustrated in Fig. 11 for a simple example of two quantum well potentials.[11] We therefore cannot use it to write the many-body Hamiltonian in the usual form $\hat{H}_0 + \hat{H}_U$. In conclusion, a basis which, as *ab-initio* Wannier functions, is complete and indeed spans the bands, is better justified, although we somewhat lose in localization.

[10] Differences in localizations between the various construction procedures are actually small for the purpose of many-body calculations, provided that the same bands are spanned with the same accuracy.

[11] Another, but less severe, problem of atomic sphere truncations is that the results will depend on the sphere size, in particular when atomic spheres are small.

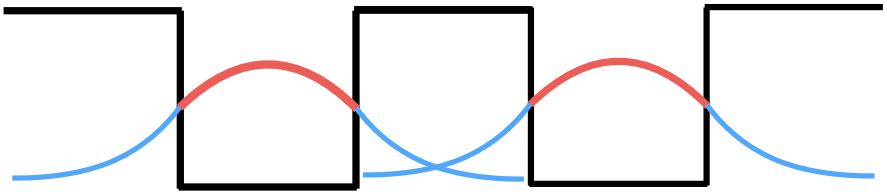

Fig. 11: *The problem of two quantum wells. The figure shows (schematically) for each well the wavefunction of a bound state. If we consider only the part of the wavefunction inside its own well (red in the figure), the differential overlap (and hence the hopping integral) between functions centered on different wells would be zero.*

3.3 Hubbard Hamiltonians for t_{2g} and e_g systems

Several strongly-correlated transition-metal oxides can be described via minimal materials-specific Hubbard-like models which involve only t_{2g} or only e_g bands. A representative system of this kind is the layered perovskite Sr_2RuO_4 with the $4d\ t_{2g}^4$ electronic configuration. Its crystal structure is shown in Fig. 12 (left side), together with the associated LDA bands crossing the Fermi level (top-right panel). Due to the layered structure the xz and yz bands are quasi one-dimensional and the xy band is quasi two-dimensional. Thus, the t_{2g} bands give rise, in first approximation, to a Fermi surface made of four crossing lines (from the xz, yz bands) and a circle (from the xy band), shown schematically in the bottom-right panel of Fig. 12. Experimentally, Sr_2RuO_4 is a correlated metal down to 1.5 K; below this temperature it becomes an anomalous superconductor. Other representative cases of t_{2g} systems are the Mott insulating perovskites $LaTiO_3$ and $YTiO_3$, with the electronic configuration $3d\ t_{2g}^1$. A paradigmatic e_g system is instead the orbitally ordered insulator $KCuF_3$, with the electronic configuration $t_{2g}^6 e_g^3$. For all these materials, if we massively downfold all LDA bands but the t_{2g} (or the e_g), the resulting 3-band (or 2-band) generalized Hubbard model takes the form

$$\begin{aligned}\hat{H} = &\sum_{i\sigma}\sum_{mm'} \varepsilon_{m,m'}\, c^\dagger_{im\sigma} c_{im'\sigma} - \sum_{\sigma}\sum_{i\neq i'}\sum_{mm'} t^{i,i'}_{m,m'}\, c^\dagger_{im\sigma} c_{i'm'\sigma} \\ &+ U \sum_{i\ m} \hat{n}_{im\uparrow}\hat{n}_{im\downarrow} + \frac{1}{2}\sum_{\substack{i\sigma\sigma' \\ m\neq m'}} \left(U - 2J - J\delta_{\sigma,\sigma'}\right) \hat{n}_{im\sigma}\hat{n}_{im'\sigma'} \\ &- J \sum_{i\ m\neq m'} \left(c^\dagger_{im\uparrow} c^\dagger_{im\downarrow} c_{im'\uparrow} c_{im'\downarrow} + c^\dagger_{im\uparrow} c_{im\downarrow} c^\dagger_{im'\downarrow} c_{im'\uparrow} \right), \end{aligned} \tag{112}$$

where $m, m' = xy, yz, xz$ for t_{2g} and $m, m' = 3z^2{-}r^2, x^2{-}y^2$ for e_g. The parameters U and J are the direct and exchange screened Coulomb integrals. The Coulomb interaction $\hat{H}_U$ is here assumed to have full $O(3)$ rotational symmetry, as in the atomic limit.[12] The first two terms of

[12] A derivation of the Coulomb interaction tensor for the free atom can be found in my chapter in Ref. [8]. There the difference in the values of U and J for the t_{2g} and e_g orbitals is also discussed.

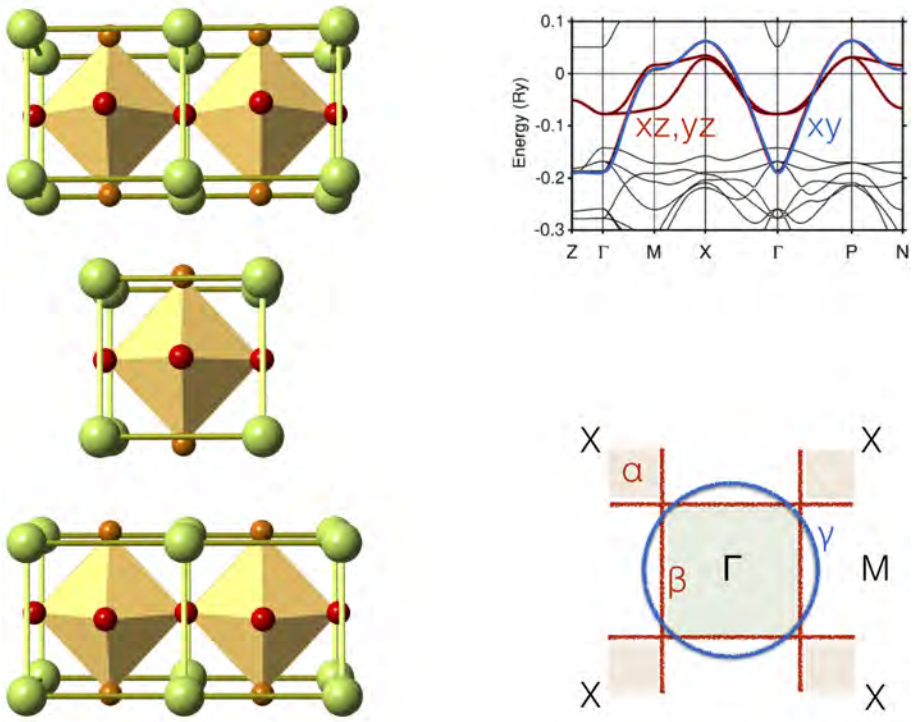

Fig. 12: *Left: Crystal structure of the tetragonal layered perovskite Sr_2RuO_4. Right: Low-energy LDA band structure (top) and schematic representation of the associated Fermi surface (bottom). The band structure was calculated using the Nth-Order Muffin-Tin Orbital (NMTO) method. The figure is rearranged from Ref. [18].*

$\hat{H}_U$ are the so-called density-density terms, and the last two are the pair-hopping and spin-flip interactions. We dropped the double-counting correction $\hat{H}_{\rm DC}$, which in this case is a mere shift of the chemical potential. The energies $\varepsilon_{m,m'}$ are the elements of the crystal-field matrix. In the case of cubic symmetry, the crystal-field matrix, the self-energy, the Green function and the spectral function are all diagonal in orbital space. For low-symmetry systems, however, this is not true. It can be seen in Fig. 13, which shows the diagonal and off-diagonal elements of the spectral-function matrix for the orthorhombic Mott insulator $YTiO_3$.

3.4 Spin-orbit interaction and effects of the basis choice

In many interesting systems the spin-orbit interaction $\hat{H}_{\rm SO}$ plays an important role. In the atomic limit, for the d shells the spin-orbit interaction is

$$\hat{H}_{\rm SO} = \sum_{\mu} \lambda_\mu \sum_{mm'} \sum_{\sigma\sigma'} \epsilon^{\mu}_{m\sigma,m'\sigma'}\, c^{\dagger}_{m\sigma} c_{m'\sigma'}, \qquad \epsilon^{\mu}_{m\sigma,m'\sigma'} = \langle m\sigma | l_\mu s_\mu | m'\sigma' \rangle, \tag{113}$$

where $\mu = x, y, z$, and λ_μ are the spin-orbit couplings, with $\lambda_\mu = \lambda$ in $O(3)$ symmetry, and

$$\lambda \sim g\mu_B^2 \left\langle \frac{1}{r}\frac{d}{dr} v_R(r) \right\rangle . \tag{114}$$

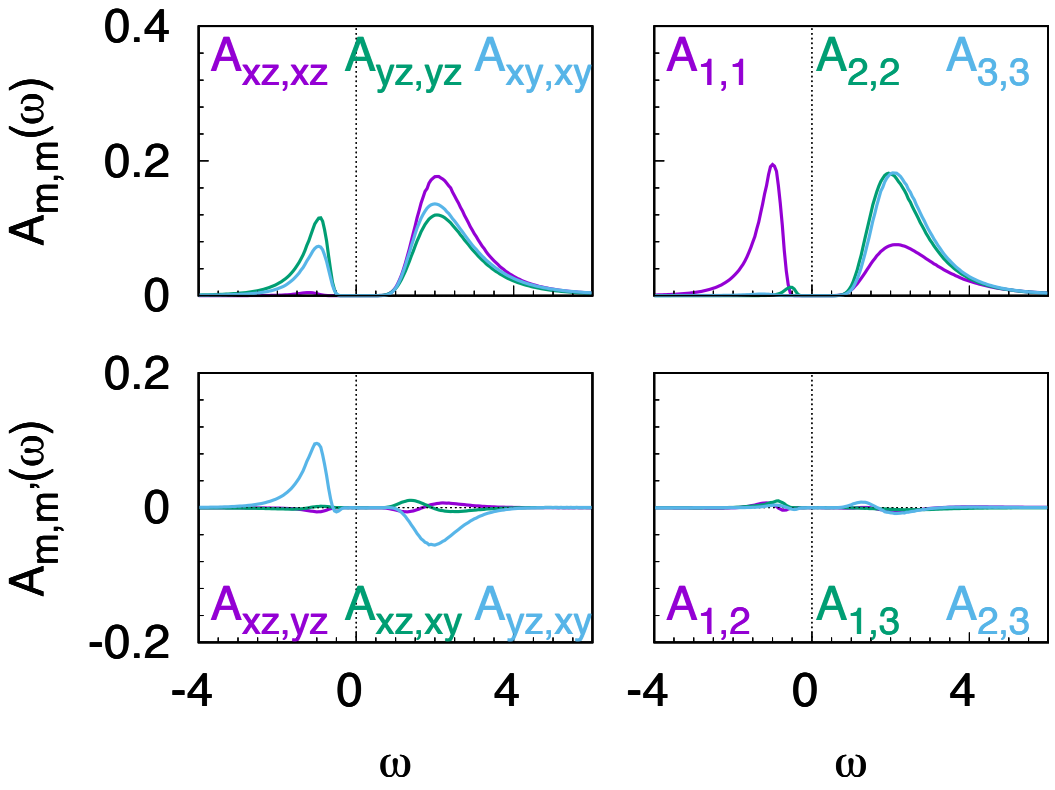

Fig. 13: *The LDA+DMFT spectral function matrix of the orbitally-ordered t_{2g}^1 system $YTiO_3$, in the (xz, yz, xy) basis (left panels) and in the crystal-field basis (right panels) [16, 19].*

For a given material, the on-site one-electron Hamiltonian is thus the matrix $\hat{\varepsilon}$ with elements $\hat{\varepsilon}_{m\sigma,m'\sigma'} = \varepsilon_{m,m'} + \sum_\mu \lambda_\mu \epsilon^\mu_{m\sigma,m'\sigma'}$, where the terms $\varepsilon_{m,m'}$ arise from the crystal field. More specifically, for a t_{2g} system with tetragonal site symmetry we have

$$\hat{\varepsilon} = \begin{pmatrix} \varepsilon_{xy} & 0 & 0 & 0 & \frac{\lambda_y}{2} & -\frac{i\lambda_x}{2} \\ 0 & \varepsilon_{yz} & \frac{i\lambda_z}{2} & -\frac{\lambda_y}{2} & 0 & 0 \\ 0 & -\frac{i\lambda_z}{2} & \varepsilon_{xz} & \frac{i\lambda_x}{2} & 0 & 0 \\ 0 & -\frac{\lambda_y}{2} & -\frac{i\lambda_x}{2} & \varepsilon_{xy} & 0 & 0 \\ \frac{\lambda_y}{2} & 0 & 0 & 0 & \varepsilon_{yz} & -\frac{i\lambda_z}{2} \\ \frac{i\lambda_x}{2} & 0 & 0 & 0 & \frac{i\lambda_z}{2} & \varepsilon_{xz} \end{pmatrix}. \tag{115}$$

Although $\hat{H}_{\rm SO}$ looks like an innocent one-body term, it turns out that, for materials, simulations including this term are more difficult. This has two reasons: (i) QMC calculations involve Green function matrices of larger size, e.g., 6×6 as in the case just discussed, hence they are from the start computationally more demanding; (ii) QMC calculations are often hampered by a much stronger sign problem; even when it can be tamed, this often happens at the price of further increasing the computational time. Thus, specific basis choices and approximations are used. A possible approach consists in working in the basis that diagonalizes the non-interacting local Green function or the non-interacting local Hamiltonian; such a choice is known to reduce

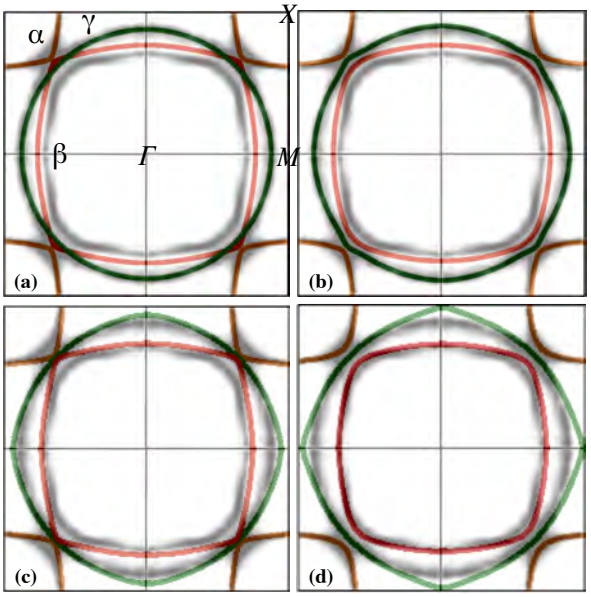

Fig. 14: *Fermi surface of Sr_2RuO_4 calculated with LDA (a), LDA+SO (b), LDA+DMFT (c) and LDA+SO+DMFT (d). Figure from [20]. The grey maps are experimental results from Ref. [23].*

the sign problem, as was first shown in Ref. [13] for the case without spin-orbit interaction. For a system with tetragonal symmetry, the states that diagonalize the local Green function belong either to the Γ_6 or to the Γ_7 irreducible representations, both 2-dimensional. There are two (coupled) Γ_7 representations, defining the space $\Gamma_7' \oplus \Gamma_7''$. The analytic expression of these states can be found in Refs. [18, 20, 21]. The transformation to the $\Gamma_6 \oplus \Gamma_7' \oplus \Gamma_7''$ basis is, of course, in principle, a mere basis change. Approximations are made, however, if all off-diagonal elements of the Green function are set to zero or the Coulomb tensor is truncated to further tame the sign problem or to reduce the computational time.

It has to be noticed that the Coulomb interaction of the t_{2g} Hubbard Hamiltonian is *only invariant under orthogonal transformations* of the basis. Thus if we change basis to the Γ_6-Γ_7'-Γ_7'' representation, the form of the interaction tensor changes. The exact expression of the Coulomb tensor in the total angular momentum basis (i.e., the one relevant when the t_{2g} crystal-field splitting is zero) can be found in Ref. [22]. For the Coulomb interaction tensor in the basis of spherical harmonics you can instead look the derivation in Ref. [8].

In the presence of crystal-field splitting, if the spin-orbit interaction is small in comparison, it is often preferable to perform the calculations in the t_{2g} basis. To this end, it is key to make QMC codes very efficient in order to reduce as much as possible statistical errors and increase the average sign. Exact LDA+SO+DMFT calculations in the t_{2g} basis have been successfully performed, e.g., for Sr_2RuO_4, using an interaction-expansion continuous-time quantum Monte Carlo solver, and an orbital-dependent phase which makes the Green function matrix real [20, 21]. This approach allowed us to study, for example, the effects of the spin-orbit interaction on the Fermi surface without approximations. The results are shown in Fig. 14 in comparison with experimental data; we will discuss them in the next section.

3.5 Non-spherical Coulomb terms and double-counting correction

While for a free atom the Coulomb tensor is spherical (symmetry $O(3)$), in a material the screened Coulomb tensor has, in general, the symmetry of the lattice. Taking into account non-spherical Coulomb terms is, in general hard, both because they make QMC calculations more difficult and can worsen the sign problem, and because in their presence the double-counting correction has to be explicitly accounted for, even when massive downfolding is used. For these reasons they are typically neglected. Recently it was shown that they can play, however, a very important role for the Fermi surface [20]. Let us therefore discuss how the double-counting correction can be treated with and without such terms, following the approach of Ref. [20]. One of the classical approximations for the double-counting correction is the so called "around mean-field" approximation. The idea is that LDA describes well the average Coulomb term, in the absence of orbital polarization. This is equivalent to using as double-counting correction the Hartree term of the Coulomb interaction tensor, i.e., the operator

$$\begin{aligned}\hat{H}_{\rm U}^{\rm DC} = & U\sum_{m}\left(\hat{n}_{m\uparrow}\bar{n}_{m\downarrow}+\bar{n}_{m\uparrow}\hat{n}_{m\downarrow}\right)+(U{-}2J)\sum_{m\neq m'}\left(\hat{n}_{m\uparrow}\bar{n}_{m'\downarrow}+\bar{n}_{m\uparrow}\hat{n}_{m'\downarrow}\right)\\ & +(U{-}3J)\sum_{\sigma}\sum_{m>m'}\left(\hat{n}_{m\sigma}\bar{n}_{m'\sigma}+\bar{n}_{m\sigma}\hat{n}_{m'\sigma}\right)-\mu\hat{N}_d \\ & -U\sum_{m}\bar{n}_{m\uparrow}\bar{n}_{m\downarrow}+(U{-}2J)\sum_{m\neq m'}\bar{n}_{m\uparrow}\bar{n}_{m'\downarrow}+(U{-}3J)\sum_{\sigma}\sum_{m>m'}\bar{n}_{m\sigma}\bar{n}_{m'\sigma}\end{aligned} \tag{116}$$

where $\bar{n}_{m\sigma} = n/d$, if n is the number of the correlated electrons per site and d the orbital degeneracy. Within this approximation we have, after collecting all terms,

$$\begin{aligned}\hat{H}_{\rm U}^{\rm DC} =& (\delta\mu{-}\mu)\hat{N}_d-\frac{n^2}{d}\big(U\,(2d{-}1)-5\,(d{-}1)\,\big)\\ \delta\mu =& \frac{n}{d}\big(U(2d{-}1)-5J(d{-}1)\big).\end{aligned}$$

If we perform massive downfolding to the correlated bands, as previously mentioned, this is merely a shift of the chemical potential and can therefore be neglected. Let us now consider the case in which the Coulomb interaction has an additional term that does not change the average U but has tetragonal symmetry

$$\Delta\hat{H}_U = \frac{\Delta U}{3}\left(2\hat{n}_{xy\uparrow}\hat{n}_{xy\downarrow}-\hat{n}_{xz\uparrow}\hat{n}_{xz\downarrow}-\hat{n}_{yz\uparrow}\hat{n}_{yz\downarrow}\right)$$

We can now use the around mean-field approximation for this term as well. We find

$$\begin{aligned}\Delta\hat{H}_U^{\rm DC} &= \frac{n}{6}\frac{\Delta U}{3}\sum_{\sigma}\left(2\hat{n}_{xy\sigma}{-}\hat{n}_{xz\sigma}{-}\hat{n}_{yz\sigma}\right)=\frac{n}{6}\Delta U\sum_{\sigma}\hat{n}_{xy\sigma}-\delta\mu'\hat{N}\\ \delta\mu' &= \frac{n}{6}\frac{\Delta U}{3}.\end{aligned}$$

This term, in addition to a shift of the chemical potential, yields an effective change of the crystal-field splitting $\varepsilon_{\rm CF}$, and has therefore to be accounted for explicitly.

How does ΔU change the Fermi surface of Sr_2RuO_4? The Fermi surface is determined by the poles of the Green function at zero frequency. These depend on the non-interacting Hamiltonian and the self-energy matrix at zero frequency. In the Fermi-liquid regime, and within the DMFT approximation, the effect of the self-energy is merely to modify the on-site part of the Hamiltonian, i.e., the crystal-field splitting $\varepsilon_{\mathrm{CF}} = \varepsilon_{xz/yz} - \varepsilon_{xy}$ and the spin-orbit couplings λ_μ

$$\varepsilon_{\mathrm{CF}} \to \varepsilon_{\mathrm{CF}} + \Delta\varepsilon_{\mathrm{CF}}(0),$$

$$\lambda_\mu \to \lambda_\mu + \Delta\lambda_\mu(0).$$

Both $\Delta\varepsilon_{\mathrm{CF}}(0)$ and $\Delta\lambda_\mu(0)$ are positive for Sr_2RuO_4, and lead to an almost doubling of the LDA parameters. The positive $\Delta\varepsilon_{\mathrm{CF}}(0)$ shrinks the β sheet (xz/yz bands) and enlarges the γ (xy band) sheet. This can be understood from the schematic Fermi surface and the LDA band structure in Fig. 12. Enhancing the crystal-field splitting corresponds to slightly moving the xy band downwards and the xz/yz bands upwards with respect to the Fermi level. The enhancement of the spin-orbit couplings has a large Hartree-Fock component [21], since the spin-orbit interaction yields a small but finite off-diagonal occupation matrix. For an $O(3)$-symmetric Coulomb tensor, the Hartree-Fock enhancement of the spin-orbit coupling is thus

$$\begin{aligned}
\frac{\Delta\lambda_z}{2} &= \quad i\big(U{-}3J\big)\, n^{\uparrow\uparrow}_{xz,yz} \\
\frac{\Delta\lambda_y}{2} &= -\,\big(U{-}3J\big)\, n^{\uparrow\downarrow}_{xy,yz}, \\
\frac{\Delta\lambda_x}{2} &= -i\big(U{-}3J\big)\, n^{\uparrow\downarrow}_{xz,xy},
\end{aligned}$$

where $n^{\sigma\sigma'}_{m,m'}$ are the off-diagonal elements of the density matrix. The Coulomb-enhanced spin-orbit coupling improves the agreement with the experimental Fermi surface at the degeneracy points (e.g., along the Γ-X direction). The agreement with ARPES data, however, further deteriorates for the γ sheet. This can be seen in Fig. 14, in which the LDA and LDA+DMFT Fermi surface are shown on top of ARPES data from Ref. [23].

Including correlation effects has thus two opposite effects: on the one hand, the agreement with experiments improves (with respect to LDA) for the β sheet; on the other hand, it deteriorates for the γ sheet. This can be seen comparing either panels (a) and (c) or panels (b) and (d) in Fig. 14. Introducing tetragonal Coulomb terms, and in particular the term ΔU, however, reduces the crystal-field enhancement to

$$\varepsilon_{\mathrm{CF}} \to \varepsilon_{\mathrm{CF}} + \Delta\varepsilon'_{\mathrm{CF}}(0),$$

where $\Delta\varepsilon'_{\mathrm{CF}}(0)$ becomes almost zero for cRPA-based estimates of ΔU. This leads to an almost perfect Fermi surface, as shown in Fig. 15. Non-spherical Coulomb terms turn out to be more important for properties that reflect the point symmetry of the lattice, like the Fermi surface, than for properties that average over orbitals, like the total spectral function [21].

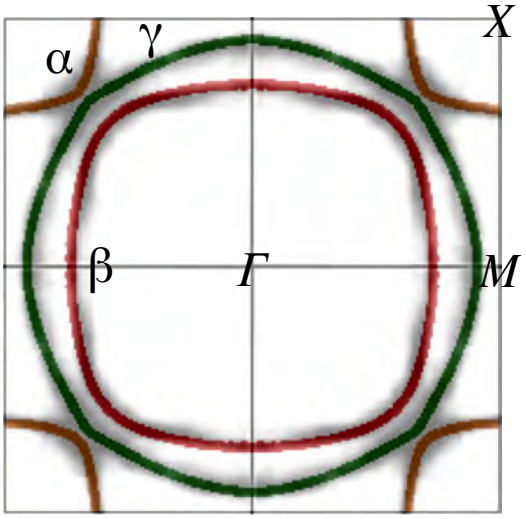

Fig. 15: *The LDA+SO+DMFT Fermi surface of Sr_2RuO_4 calculated including the effects of the non-spherical Coulomb term ΔU. Figure from [20].*

4 Understanding correlated materials with DMFT

The ultimate test for a method is the actual advance it brings in solving outstanding problems. The LDA+DMFT approach has proven very successful, advancing qualitatively our understanding of the physics of strongly-correlated materials. This has two reasons. From the many-body side, the success of the method is rooted in the fact that dynamical mean-field theory captures exactly key limits: non-interacting limit, atomic limit, single-impurity limit, infinite dimension limit. It also describes very well phases with different characteristics: paramagnetism, long-range order, metallic and insulating phase. Thus DMFT can be used to explore transitions/crossovers from one corner to another of the phase diagram, building a coherent picture as a function of both internal and external parameters (e.g., U, J, doping and temperature). This differs from static mean-field approaches, such as the LDA+U method; the latter only captures the behavior in a specific corner of the phase diagram (and typically merely the ground state), e.g., long-range magnetic order[13] or, if one uses large supercells, spin-glass-like phases. This limitation makes static mean-field approaches unsuitable to study, e.g., the effects of temperature or external parameters, and for identifying a mechanism behind a certain phenomenon, or finding the onset of a Mott phase. From the materials-dependence side, by constructing many-body models from Kohn-Sham Wannier functions, the LDA+DMFT technique builds on the shoulders of the most successful theory for materials, DFT. In order to illustrate the success of LDA+DMFT, here I will briefly review two paradigmatic examples.

[13] It should be noted that LDA+U is less accurate than DMFT also in capturing long-range order. This is because LDA+U is based on the Hartree-Fock approximation; as we have seen for the Hubbard dimer, it is, therefore, the static (high-frequency) limit of LDA+DMFT. All results from LDA+U are thus by construction contained in LDA+DMFT, provided that, of course, calculations are performed for the same Hamiltonian, the same basis and the same unit cell. Unlike LDA+U, however, LDA+DMFT also captures correctly dynamical fluctuations and actual phase transitions. See Ref. [14] for more details. Long-range order is well described in DMFT via a local cluster with the size of the (enlarged) broken-symmetry unit cell, without additional computational cost.

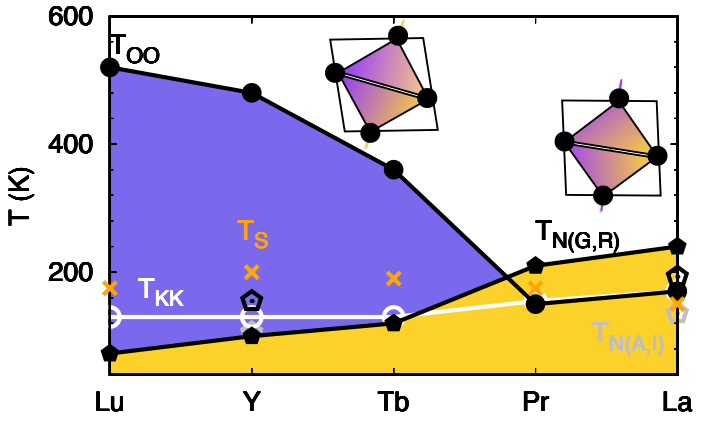

Fig. 16: *Inversion of magnetic and orbital transition in the $ReVO_3$ series with increasing rare-earth (Re) ionic radius. While in most orbitally ordered systems the magnetic transition occurs at lower temperature than the orbital transition (T_N<T_{OO}), in the $ReVO_3$ series $T_N \gtrsim T_{OO}$ for large rare-earth (Re) radius. Figure from [35].*

The first is unravelling the importance of **crystal-field splitting** in determining low-energy properties of strongly-correlated systems. The metal-insulator Mott transition arises, in the simplest picture, from the competition between the bandwidth, W, and the on-site Coulomb repulsion, U. This competition is well captured by the single-band Hubbard model; however, the latter is typically insufficient for understanding the complex behavior displayed by actual correlated materials. One reason is the importance of multi-orbital effects. Pioneering works based on lattice QMC calculations for the multi-band Hubbard model have indeed shown that orbital degeneracy strongly influence the size of the Mott gap [24, 25]. Accounting for multi-orbital effects strongly complicates the matter from the viewpoint of theory: realistic models have many unknown independent parameters and are considerably more difficult to solve. The LDA+DMFT approach provided the first framework to study multi-orbital phenomena systematically in a realistic setting. One of the early success of the method was to show that, contrarily to what was often assumed, small details do matter. A crystal-field splitting much smaller than the bandwidth can favor the Mott metal-insulator transition. In fact, everything else remaining the same, the crystal-field splitting reduces orbital degeneracy, thereby modifying the correlation strength. This insight explained the metal-insulator transition in the series of $3d^1$ perovskites: $SrVO_3$ (metal), $CaVO_3$ (metal), $LaTiO_3$ (small gap insulator), $YTiO_3$ (insulator) [19]. Important crystal-field effects are now recognized in most correlated materials. They have been key to settle several hot debates, e.g., to understand the complex phase diagram of layered $Ca_{2-x}Sr_xRuO_4$ ruthenates [26]. More recently, it was shown that the crystal-field splitting and its subtle interplay with the **spin-orbit interaction** is crucial for determining the correlation strength, the shape of the Fermi surface and the effective masses [20–22, 27].

The second success story is unravelling the **origin of orbital ordering** in materials. More than fifty years ago, thanks to seminal works of Kugel and Khomskii [28], it became clear that orbital degrees of freedom play a key role in the properties of strongly-correlated Mott insulators; in particular, they can give rise to orbital ordering via many-body super-exchange interactions [29,

30]. For a long time it was however hotly debated if, in actual materials, it is Kugel-Khomskii (KK) super-exchange or rather the Jahn-Teller effect that control the onset of orbital ordering. This is a classical case of a chicken-and-egg problem, with two theoretical mechanisms leading to the same final state. The systems for which super-exchange-driven orbital ordering was initially proposed were the e_g perovskites $KCuF_3$ and $LaMnO_3$. Combining DMFT with a novel disentanglement scheme [31], it became possible to solve the problem. It was shown that, in $KCuF_3$ and $LaMnO_3$, the KK super-exchange interaction, although strong, is not sufficiently large to drive alone orbital ordering at experimental temperatures [31, 32]. More recently, it was shown that t_{2g} systems are more likely than e_g materials to exhibit super-exchange-driven orbital ordering; $LaVO_3$ was then identified as the first clear-cut case of a Kugel-Khomskii material [33, 34]. This lead to the solution of another long-standing problem: the origin of the puzzling inversion of magnetic and orbital transition in the $ReVO_3$ series with increasing rare-earth (Re) ionic radius, see Fig. 16 and Refs. [34, 35]. Furthermore, as a byproduct, it was shown that DMFT and super-exchange theory can be successfully combined to pinpoint the nature of spin-orbital phases. This can be done via a general scheme for constructing **exact materials-specific super-exchange Hamiltonians** in an irreducible tensor basis [33–35]; the latter provides at the same time analytic expressions and numerical results. This scheme can be used for the realistic description of all KK-type super-exchange phenomena, static (e.g., orbital ordering) and dynamical (e.g., spin-orbital excitations, orbital and spin liquid behavior).

5 Conclusion and outlook

The LDA+DMFT approach and its extension has proven very successful for describing correlated materials. In the last decades, it also became very versatile. It is now possible, e.g., to study multi-orbital models including the full Coulomb vertex and the spin-orbit interaction, and to calculate response functions or bosonic excitations. Still, several challenges remain. Models with more than a few orbitals or sites and out-of-equilibrium phenomena are still, e.g., hard to study. Furthermore, since the birth of DFT, Moore's law constantly helped as much as new algorithms in extending the frontier; that has come now slowly to a halt.

Quantum computers and artificial intelligence, or new, not yet foreseeable, technological advances might help us in the future. The present deceleration, however, urges us to think to what we should strive for. It is perhaps easier to discuss first what we *do not* need. We do not need a magical calculating machine that gives us answers with no explanations. Reproducing the data is, of course, the aim of theory, but not the only goal. As scientists we need to know why. The danger of giving this question up is evident if we look back at the historical controversy between copernican and ptolemaic system. At the time, the ptolemaic system was the one which agreed better with experiments. Indeed, it had been fine-tuned along the years, via a series of ad hoc assumptions. The copernican system was initially not performing so well, among others because it was based on circular orbits. But, at the end, it is the copernican system that made a contribution to science, by identifying the correct picture.

Appendices

A Hubbard dimer and Anderson molecule

The Hamiltonian of the **Hubbard dimer** is given by

$$\hat{H} = \varepsilon_d \sum_{\sigma} \sum_{i=1,2} n_{i\sigma} - t \sum_{\sigma} \left(c^{\dagger}_{1\sigma} c_{2\sigma} + c^{\dagger}_{2\sigma} c_{1\sigma} \right) + U \sum_{i=1,2} \hat{n}_{i\uparrow} \hat{n}_{i\downarrow}.$$

It commutes with the number of electron operator $\hat{N}$, with the total spin $\hat{S}$, and with $\hat{S}_z$. Thus we can express the many-body states in the atomic limit as

$\lvert N, S, S_z \rangle$			N	S	$E(N,S)$
$\lvert 0,0,0 \rangle$	$=$	$\lvert 0 \rangle$	0	0	0
$\lvert 1, \frac{1}{2}, \sigma \rangle_1$	$=$	$c^{\dagger}_{1\sigma} \lvert 0 \rangle$	1	$\frac{1}{2}$	ε_d
$\lvert 1, \frac{1}{2}, \sigma \rangle_2$	$=$	$c^{\dagger}_{2\sigma} \lvert 0 \rangle$	1	$\frac{1}{2}$	ε_d
$\lvert 2,1,1 \rangle$	$=$	$c^{\dagger}_{2\uparrow} c^{\dagger}_{1\uparrow} \lvert 0 \rangle$	2	1	$2\varepsilon_d$
$\lvert 2,1,-1 \rangle$	$=$	$c^{\dagger}_{2\downarrow} c^{\dagger}_{1\downarrow} \lvert 0 \rangle$	2	1	$2\varepsilon_d$
$\lvert 2,1,0 \rangle$	$=$	$\frac{1}{\sqrt{2}} \left(c^{\dagger}_{1\uparrow} c^{\dagger}_{2\downarrow} + c^{\dagger}_{1\downarrow} c^{\dagger}_{2\uparrow} \right) \lvert 0 \rangle$	2	1	$2\varepsilon_d$
$\lvert 2,0,0 \rangle_0$	$=$	$\frac{1}{\sqrt{2}} \left(c^{\dagger}_{1\uparrow} c^{\dagger}_{2\downarrow} - c^{\dagger}_{1\downarrow} c^{\dagger}_{2\uparrow} \right) \lvert 0 \rangle$	2	0	$2\varepsilon_d$
$\lvert 2,0,0 \rangle_1$	$=$	$c^{\dagger}_{1\uparrow} c^{\dagger}_{1\downarrow} \lvert 0 \rangle$	2	0	$2\varepsilon_d + U$
$\lvert 2,0,0 \rangle_2$	$=$	$c^{\dagger}_{2\uparrow} c^{\dagger}_{2\downarrow} \lvert 0 \rangle$	2	0	$2\varepsilon_d + U$
$\lvert 3, \frac{1}{2}, \sigma \rangle_1$	$=$	$c^{\dagger}_{1\sigma} c^{\dagger}_{2\uparrow} c^{\dagger}_{2\downarrow} \lvert 0 \rangle$	3	$\frac{1}{2}$	$3\varepsilon_d + U$
$\lvert 3, \frac{1}{2}, \sigma \rangle_2$	$=$	$c^{\dagger}_{2\sigma} c^{\dagger}_{1\uparrow} c^{\dagger}_{1\downarrow} \lvert 0 \rangle$	3	$\frac{1}{2}$	$3\varepsilon_d + U$
$\lvert 4,0,0 \rangle$	$=$	$c^{\dagger}_{1\uparrow} c^{\dagger}_{1\downarrow} c^{\dagger}_{2\uparrow} c^{\dagger}_{2\downarrow} \lvert 0 \rangle$	4	0	$4\varepsilon_d + 2U$

Let us order the $N = 1$ states as in the table above, first the spin up and then spin down block. For finite t the Hamiltonian matrix for $N = 1$ electrons takes then the form

$$\hat{H}_1 = \begin{pmatrix} \varepsilon_d & -t & 0 & 0 \\ -t & \varepsilon_d & 0 & 0 \\ 0 & 0 & \varepsilon_d & -t \\ 0 & 0 & -t & \varepsilon_d \end{pmatrix}.$$

This matrix can be easily diagonalized and yields the *bonding* $(-)$ and *antibonding* $(+)$ states

$\|1,S,S_z\rangle_\alpha$		$E_\alpha(1,S)$	$d_\alpha(1,S)$
$\|1,\frac{1}{2},\sigma\rangle_+$	$= \frac{1}{\sqrt{2}}\big(\|1,\frac{1}{2},\sigma\rangle_1 - \|1,\frac{1}{2},\sigma\rangle_2\big)$	$\varepsilon_d + t$	2
$\|1,\frac{1}{2},\sigma\rangle_-$	$= \frac{1}{\sqrt{2}}\big(\|1,\frac{1}{2},\sigma\rangle_1 + \|1,\frac{1}{2},\sigma\rangle_2\big)$	$\varepsilon_d - t$	2

where $d_\alpha(N)$ is the spin degeneracy of the α manifold.
For $N = 2$ electrons (half filling), the hopping integrals only couple the three $S = 0$ states, and therefore the Hamiltonian matrix is given by

$$\hat{H}_2 = \begin{pmatrix} 2\varepsilon_d & 0 & 0 & 0 & 0 & 0 \\ 0 & 2\varepsilon_d & 0 & 0 & 0 & 0 \\ 0 & 0 & 2\varepsilon_d & 0 & 0 & 0 \\ 0 & 0 & 0 & 2\varepsilon_d & -\sqrt{2}t & -\sqrt{2}t \\ 0 & 0 & 0 & -\sqrt{2}t & 2\varepsilon_d{+}U & 0 \\ 0 & 0 & 0 & -\sqrt{2}t & 0 & 2\varepsilon_d{+}U \end{pmatrix}.$$

The eigenvalues and the corresponding eigenvectors are

$\|2,S,S_z\rangle_\alpha$		$E_\alpha(2,S)$	$d_\alpha(2,S)$
$\|2,0,0\rangle_+$	$= a_1\|2,0,0\rangle_0 - \frac{a_2}{\sqrt{2}}\big(\|2,0,0\rangle_1 + \|2,0,0\rangle_2\big)$	$2\varepsilon_d + \frac{1}{2}\,(U{+}\Delta(t,U))$	1
$\|2,0,0\rangle_o$	$= \frac{1}{\sqrt{2}}\big(\|2,0,0\rangle_1 - \|2,0,0\rangle_2\big)$	$2\varepsilon_d + U$	1
$\|2,1,m\rangle_o$	$= \|2,1,m\rangle$	$2\varepsilon_d$	3
$\|2,0,0\rangle_-$	$= a_2\|2,0,0\rangle_0 + \frac{a_1}{\sqrt{2}}\big(\|2,0,0\rangle_1 + \|2,0,0\rangle_2\big)$	$2\varepsilon_d + \frac{1}{2}\,(U{-}\Delta(t,U))$	1

where

$$\Delta(t,U) = \sqrt{U^2 + 16t^2},$$

and

$$a_1^2 = a_1^2(t,U) = \frac{1}{\Delta(t,U)}\frac{\Delta(t,U) - U}{2} \qquad a_2^2 = a_2^2(t,U) = \frac{4t^2}{\Delta(t,U)}\frac{2}{\Delta(t,U) - U}\,,$$

so that $a_1 a_2 = 2t/\Delta(t,U)$. For $U = 0$ we have $a_1 = a_2 = 1/\sqrt{2}$, and the two states $|2,0,0\rangle_-$ and $|2,0,0\rangle_+$ become, respectively, the state with two electrons in the bonding orbital and the state with two electrons in the antibonding orbital; they have energy $E_\pm(2,0) = 2\varepsilon_d \pm 2t$; the remaining states have energy $2\varepsilon_d$ and are non-bonding. For $t > 0$, the ground state is unique and it is always the singlet $|2,0,0\rangle_-$; in the large U limit its energy is

$$E_-(2,0) \sim 2\varepsilon_d - 4t^2/U.$$

In this limit the energy difference between the first excited state, a triplet state, and the singlet ground state is thus equal to the Heisenberg antiferromagnetic coupling

$$E_o(2,1) - E_-(2,0) \sim 4t^2/U = \Gamma.$$

Finally, for $N = 3$ electrons, eigenstates and eigenvectors are

$\lvert 3, S, S_z\rangle_\alpha$		$E_\alpha(3)$	$d_\alpha(3,S)$
$\lvert 3, \frac{1}{2}, \sigma\rangle_+$	$= \frac{1}{\sqrt{2}}\big(\lvert 1, \frac{1}{2}, \sigma\rangle_1 + \lvert 1, \frac{1}{2}, \sigma\rangle_2\big)$	$3\varepsilon_d{+}U + t$	2
$\lvert 3, \frac{1}{2}, \sigma\rangle_-$	$= \frac{1}{\sqrt{2}}\big(\lvert 1, \frac{1}{2}, \sigma\rangle_1 - \lvert 1, \frac{1}{2}, \sigma\rangle_2\big)$	$3\varepsilon_d{+}U - t$	2

If we exchange holes and electrons, the $N{=}3$ case is identical to the $N{=}1$ electron case. This is due to the particle-hole symmetry of the model.

The Hamiltonian of the **Anderson molecule** is given by

$$\hat{H} = \varepsilon_s \sum_\sigma \hat{n}_{2\sigma} - t \sum_\sigma \left(c^\dagger_{1\sigma} c_{2\sigma} + c^\dagger_{2\sigma} c_{1\sigma}\right) + \varepsilon_d \sum_\sigma \hat{n}_{1\sigma} + U \hat{n}_{1\uparrow}\hat{n}_{1\downarrow}.$$

In the atomic limit, its eigenstates states can be classified as

$\lvert N, S, S_z\rangle$			N	S	$E(N,S)$
$\lvert 0,0,0\rangle$	$=$	$\lvert 0\rangle$	0	0	0
$\lvert 1, \frac{1}{2}, \sigma\rangle_1$	$=$	$c^\dagger_{1\sigma}\lvert 0\rangle$	1	$\frac{1}{2}$	ε_d
$\lvert 1, \frac{1}{2}, \sigma\rangle_2$	$=$	$c^\dagger_{2\sigma}\lvert 0\rangle$	1	$\frac{1}{2}$	ε_s
$\lvert 2,1,1\rangle$	$=$	$c^\dagger_{2\uparrow}c^\dagger_{1\uparrow}\lvert 0\rangle$	2	1	$\varepsilon_d + \varepsilon_s$
$\lvert 2,1,-1\rangle$	$=$	$c^\dagger_{2\downarrow}c^\dagger_{1\downarrow}\lvert 0\rangle$	2	1	$\varepsilon_d + \varepsilon_s$
$\lvert 2,1,0\rangle$	$=$	$\frac{1}{\sqrt{2}}\big(c^\dagger_{1\uparrow}c^\dagger_{2\downarrow} + c^\dagger_{1\downarrow}c^\dagger_{2\uparrow}\big)\lvert 0\rangle$	2	1	$\varepsilon_d + \varepsilon_s$
$\lvert 2,0,0\rangle_0$	$=$	$\frac{1}{\sqrt{2}}\big(c^\dagger_{1\uparrow}c^\dagger_{2\downarrow} - c^\dagger_{1\downarrow}c^\dagger_{2\uparrow}\big)\lvert 0\rangle$	2	0	$\varepsilon_d + \varepsilon_s$
$\lvert 2,0,0\rangle_1$	$=$	$c^\dagger_{1\uparrow}c^\dagger_{1\downarrow}\lvert 0\rangle$	2	0	$2\varepsilon_d + U$
$\lvert 2,0,0\rangle_2$	$=$	$c^\dagger_{2\uparrow}c^\dagger_{2\downarrow}\lvert 0\rangle$	2	0	$2\varepsilon_s$
$\lvert 3, \frac{1}{2}, \sigma\rangle_1$	$=$	$c^\dagger_{1\sigma}c^\dagger_{2\uparrow}c^\dagger_{2\downarrow}\lvert 0\rangle$	3	$\frac{1}{2}$	$\varepsilon_d + 2\varepsilon_s$
$\lvert 3, \frac{1}{2}, \sigma\rangle_2$	$=$	$c^\dagger_{2\sigma}c^\dagger_{1\uparrow}c^\dagger_{1\downarrow}\lvert 0\rangle$	3	$\frac{1}{2}$	$2\varepsilon_d + \varepsilon_s + U$
$\lvert 4,0,0\rangle$	$=$	$c^\dagger_{1\uparrow}c^\dagger_{1\downarrow}c^\dagger_{2\uparrow}c^\dagger_{2\downarrow}\lvert 0\rangle$	4	0	$2\varepsilon_d + 2\varepsilon_s + U$

For $N = 1$ electrons the Hamiltonian can be written in the matrix form

$$\hat{H}_1 = \begin{pmatrix} \varepsilon_d & -t & 0 & 0 \\ -t & \varepsilon_s & 0 & 0 \\ 0 & 0 & \varepsilon_d & -t \\ 0 & 0 & -t & \varepsilon_s \end{pmatrix}.$$

The eigenstates are thus

$\|1, S, S_z\rangle_\alpha$	$E_\alpha(1, S)$	$d_\alpha(1, S)$
$\|1, \frac{1}{2}, \sigma\rangle_+ = \alpha_1 \|1, \frac{1}{2}, \sigma\rangle_1 - \alpha_2 \|1, \frac{1}{2}, \sigma\rangle_2$	$\frac{1}{2}\big(\varepsilon_d + \varepsilon_s + \sqrt{(\varepsilon_d - \varepsilon_s)^2 + 4t^2}\big)$	2
$\|1, \frac{1}{2}, \sigma\rangle_- = \alpha_2 \|1, \frac{1}{2}, \sigma\rangle_1 + \alpha_1 \|1, \frac{1}{2}, \sigma\rangle_2$	$\frac{1}{2}\big(\varepsilon_d + \varepsilon_s - \sqrt{(\varepsilon_d - \varepsilon_s)^2 + 4t^2}\big)$	2

where $d_\alpha(N)$ is the spin degeneracy of the α manifold. For $\varepsilon_s = \varepsilon_d + U/2$ the eigenvalues are

$$E_\pm(1, S) = \varepsilon_d + \frac{1}{4}\big(U \pm \Delta(U, t)\big),$$

while the coefficients are $\alpha_1 = a_1(t, U)$ and $\alpha_2 = a_2(t, U)$.
For N=2 electrons, the hopping integrals only couple the S=0 states. The Hamiltonian is

$$\hat{H}_2 = \begin{pmatrix} \varepsilon_d{+}\varepsilon_s & 0 & 0 & 0 & 0 & 0 \\ 0 & \varepsilon_d{+}\varepsilon_s & 0 & 0 & 0 & 0 \\ 0 & 0 & \varepsilon_d{+}\varepsilon_s & 0 & 0 & 0 \\ 0 & 0 & 0 & \varepsilon_d{+}\varepsilon_s & -\sqrt{2}t & -\sqrt{2}t \\ 0 & 0 & 0 & -\sqrt{2}t & 2\varepsilon_d{+}U & 0 \\ 0 & 0 & 0 & -\sqrt{2}t & 0 & 2\varepsilon_s \end{pmatrix}$$

For $\varepsilon_s = \varepsilon_d + U/2$ the eigenvalues and the corresponding eigenvectors are

$\|2, S, S_z\rangle_\alpha$	$E_\alpha(2, S)$	$d_\alpha(2, S)$
$\|2,0,0\rangle_+ = b_1 \|2,0,0\rangle_0 - \frac{b_2}{\sqrt{2}}\big(\|2,0,0\rangle_1 + \|2,0,0\rangle_2\big)$	$2\varepsilon_d + \frac{U}{2} + \frac{1}{4}\big(U{+}2\Delta(t, \frac{U}{2})\big)$	1
$\|2,0,0\rangle_o = \frac{1}{\sqrt{2}}\big(\|2,0,0\rangle_1 - \|2,0,0\rangle_2\big)$	$2\varepsilon_d + U$	1
$\|2,1,m\rangle_o = \|2,1,m\rangle$	$2\varepsilon_d + \frac{U}{2}$	3
$\|2,0,0\rangle_- = b_2 \|2,0,0\rangle_0 + \frac{b_1}{\sqrt{2}}\big(\|2,0,0\rangle_1 + \|2,0,0\rangle_2\big)$	$2\varepsilon_d + \frac{U}{2} + \frac{1}{4}\big(U{-}2\Delta(t, \frac{U}{2})\big)$	1

where $b_1 = a_1(t, U/2)$ and $b_2 = a_2(t, U/2)$. These states have the same form as in the case of the Hubbard dimer; the ground state energy and the weight of doubly occupied states in $|2, 0, 0\rangle_-$ differ, however. Finally, for $N = 3$ electrons, the eigenstates are

$\|3, S, S_z\rangle_\alpha$	$E_\alpha(3, S)$	$d_\alpha(3, S)$
$\|3, \frac{1}{2}, \sigma\rangle_+ = \alpha_2 \|1, \frac{1}{2}, \sigma\rangle_1 + \alpha_1 \|1, \frac{1}{2}, \sigma\rangle_2$	$3\varepsilon_d + U + \frac{1}{4}\big(U{+}\Delta(t, U)\big)$	2
$\|3, \frac{1}{2}, \sigma\rangle_- = \alpha_1 \|1, \frac{1}{2}, \sigma\rangle_1 - \alpha_2 \|1, \frac{1}{2}, \sigma\rangle_2$	$3\varepsilon_d + U + \frac{1}{4}\big(U{-}\Delta(t, U)\big)$	2

B Lehmann representation of the local Green function

For a single-orbital model, the local Matsubara Green function for a given site i is defined as

$$G^{\sigma}_{i,i}(i\nu_n) = -\int_0^{\beta} d\tau\, e^{i\nu_n\tau}\big\langle \mathcal{T} c_{i\sigma}(\tau)c^{\dagger}_{i\sigma}(0)\big\rangle, \tag{117}$$

where $\mathcal{T}$ is the time-ordering operator, $\beta = 1/k_BT$, and ν_n a fermionic Matsubara frequency. Let us assume to know all eigenstates $|N_l\rangle$ and their energy $E_l(N)$, for arbitrary number of electrons N. Thus, formally

$$G^{\sigma}_{i,i}(i\nu_n) = -\frac{1}{Z}\sum_{Nl}\int_0^{\beta} d\tau\, e^{i\nu_n\tau}e^{-\Delta E_l(N)\beta}\langle N_l|c_{i\sigma}(\tau)c^{\dagger}_{i\sigma}(0)|N_l\rangle, \tag{118}$$

where $Z = \sum_{Nl} e^{-\Delta E_l(N)\beta}$ is the partition function, $\Delta E_l(N){=}E_l(N){-}\mu N$ with μ the chemical potential, and $c^{\dagger}_{i\sigma}(0) = c^{\dagger}_{i\sigma}$. We now insert a complete set of states, obtaining

$$\begin{aligned} G^{\sigma}_{i,i}(i\nu_n) &= -\frac{1}{Z}\sum_{ll'NN'}\int_0^{\beta} d\tau\, e^{i\nu_n\tau}e^{-\Delta E_l(N)\beta}\langle N_l|c_{i\sigma}(\tau)|N'_{l'}\rangle\langle N'_{l'}|c^{\dagger}_{i\sigma}|N_l\rangle \\ &= -\frac{1}{Z}\sum_{ll'NN'}\int_0^{\beta} d\tau\, e^{-\Delta E_l(N)\beta}e^{(i\nu_n+\Delta E_l(N)-\Delta E_{l'}(N'))\tau}\left|\langle N'_{l'}|c^{\dagger}_{i\sigma}|N_l\rangle\right|^2 \\ &= \frac{1}{Z}\sum_{ll'NN'}\frac{e^{-\Delta E_{l'}(N')\beta}+e^{-\Delta E_l(N)\beta}}{i\nu_n+\Delta E_l(N){-}\Delta E_{l'}(N')}\left|\langle N'_{l'}|c^{\dagger}_{i\sigma}|N_l\rangle\right|^2. \end{aligned} \tag{119}$$

Due to the weight $\left|\langle N'_{l'}|c^{\dagger}_{i\sigma}(0)|N_l\rangle\right|^2$ only the terms for which $N' = N{+}1$ contribute. Thus, after exchanging the labels $l'N' \leftrightarrow lN$ in the first addend, we obtain the Lehmann representation

$$G^{\sigma}_{i,i}(i\nu_n){=}\sum_{ll'N}\frac{e^{-\beta\Delta E_l(N)}}{Z}\left(\frac{\left|\langle(N{-}1)_{l'}|c_{i\sigma}|N_l\rangle\right|^2}{i\nu_n-\Delta E_l(N){+}\Delta E_{l'}(N{-}1)}{+}\frac{\left|\langle(N{+}1)_{l'}|c^{\dagger}_{i\sigma}|N_l\rangle\right|^2}{i\nu_n-\Delta E_{l'}(N{+}1){+}\Delta E_l(N)}\right).$$

Let us consider as example the atomic limit of the Hubbard model at half filling (for which $\mu{=}\varepsilon_d{+}U/2$). In this case all sites are decoupled; there are four eigenstates per site, the vacuum $|0\rangle$, with $\Delta E(0) = 0$, the doublet $|1_\sigma\rangle = c^{\dagger}_{i\sigma}|0\rangle$, with $\Delta E_\sigma(1) = -U/2$, and the doubly-occupied singlet $|2\rangle = c^{\dagger}_{i\uparrow}c^{\dagger}_{i\downarrow}|0\rangle$, with $\Delta E(2) = 0$. Furthermore, $Z = 2\big(1+e^{\beta U/2}\big)$ and

$$\left|\langle(N{-}1)_{l'}|c_{i\sigma}|N_l\rangle\right|^2{=}\begin{cases}1 & \text{if } |N_l\rangle{=}|2\rangle\vee|1_\sigma\rangle\\ 0 & \text{otherwise}\end{cases}\qquad \left|\langle(N{+}1)_{l'}|c^{\dagger}_{i\sigma}|N_l\rangle\right|^2{=}\begin{cases}1 & \text{if } |N_l\rangle{=}|0\rangle\vee|1_{-\sigma}\rangle\\ 0 & \text{otherwise}\end{cases}$$

Thus, after summing up the four non-zero contributions, we find

$$G^{\sigma}_{i,i}(\nu_n) = \frac{1}{2}\left(\frac{1}{i\nu_n+U/2}+\frac{1}{i\nu_n-U/2}\right). \tag{120}$$

References

[1] P. Hohenberg and W. Kohn, Phys. Rev. **136**, B864 (1964);
W. Kohn and L.J. Sham, Phys. Rev. **140**, A1133 (1965)

[2] W. Kohn, Rev. Mod. Phys. **71**, 1253 (1999)

[3] P.W. Anderson: *More and different – Notes from a thoughtful curmudgeon*
(World Scientific, Singapore, 2011)

[4] W. Metzner and D. Vollhardt, Phys. Rev. Lett. **62**, 324 (1989)

[5] E. Müller-Hartmann, Z. Phys. B **74**, 507 (1989);
Z. Phys. B **76**, 211 (1989); Int. J. Mod. Phys. B **3**, 2169 (1989)

[6] A. Georges and G. Kotliar, Phys. Rev. B **45**, 6479 (1992)

[7] M. Jarrell, Phys. Rev. Lett. **69**, 168 (1992)

[8] E. Pavarini, E. Koch, D. Vollhardt, A. Lichtenstein (eds.):
The LDA+DMFT approach to strongly-correlated materials,
Reihe Modeling and Simulation, Vol. 1 (Forschungszentrum Jülich, 2011)
`http://www.cond-mat.de/events/correl11`

[9] E. Pavarini, E. Koch, A. Lichtenstein, D. Vollhardt (eds.):
DMFT at 25: Infinite dimensions,
Reihe Modeling and Simulation, Vol. 4 (Forschungszentrum Jülich, 2014)
`http://www.cond-mat.de/events/correl14`

[10] E. Pavarini, E. Koch, A. Lichtenstein, D. Vollhardt (eds.):
DMFT: From infinite dimensions to real materials,
Reihe Modeling and Simulation, Vol. 8 (Forschungszentrum Jülich, 2018)
`http://www.cond-mat.de/events/correl18`

[11] E. Koch, G. Sangiovanni, and O. Gunnarsson, Phys. Rev. B **78**, 115102 (2008)

[12] E. Gull, A.J. Millis, A.I. Lichtenstein, A.N. Rubtsov, M. Troyer, and P. Werner,
Rev. Mod. Phys. **83**, 349 (2011)

[13] A. Flesch, E. Gorelov, E. Koch, E. Pavarini, Phys. Rev. B **87**, 195141 (2013)

[14] E. Pavarini, E. Koch, R. Scalettar, and R.M. Martin (eds.):
The physics of correlated insulators, metals, and superconductors
Reihe Modeling and Simulation, Vol. 7 (Forschungszentrum Jülich, 2017)
`http://www.cond-mat.de/events/correl17`

[15] A. Kiani and E. Pavarini, Phys. Rev. B **94**, 075112 (2016)

[16] E. Pavarini, A. Yamasaki, J. Nuss, and O.K. Andersen,
New. J. Phys **7**, 188 (2005)

[17] N. Marzari, A.A. Mostofi, J.R. Yates, I. Souza, and D. Vanderbilt,
Rev. Mod. Phys. **84**, 1419 (2012)

[18] G. Zhang and E. Pavarini, Phys. Status Solidi RRL **12**, 1800211 (2018)

[19] E. Pavarini, S. Biermann, A. Poteryaev, A.I. Lichtenstein, A. Georges, and O.K. Andersen,
Phys. Rev. Lett. **92**, 176403 (2004)

[20] G. Zhang, E. Gorelov, E. Sarvestani, and E. Pavarini, Phys. Rev. Lett. **116**, 106402 (2016)

[21] E. Sarvestani, G. Zhang, E. Gorelov, and E. Pavarini, Phys. Rev. B **97**, 085141 (2018)

[22] G. Zhang and E. Pavarini, Phys. Rev. B **99**, 125102 (2019)

[23] A. Damascelli, D.H. Lu, K.M. Shen, N.P. Armitage, F. Ronning, D.L. Feng, C. Kim,
Z.-X. Shen, T. Kimura, Y. Tokura, Z.Q. Mao, and Y. Maeno,
Phys. Rev. Lett. **85**, 5194 (2000)

[24] O. Gunnarsson, E. Koch, and R.M. Martin, Phys. Rev. B **56**, 1146 (1996)

[25] E. Koch, O. Gunnarsson, and R.M. Martin, Phys. Rev. B **60**, 15714 (1999)

[26] E. Gorelov, M. Karolak, T.O. Wehling, F. Lechermann, A.I. Lichtenstein, E. Pavarini,
Phys. Rev. Lett. **104**, 226401 (2010)

[27] N. Samani, G. Zhang and E. Pavarini, Phys. Rev. Lett. **132**, 236505 (2024)

[28] K.I. Kugel and D.I. Khomskii, Zh. Eksp. Teor. Fiz. **64**, 1429 (1973)
[Sov. Phys. JETP **37**, 725 (1973)]

[29] D.I. Khomskii, *Transition metal compounds*, Cambridge University Press (2014)

[30] E. Pavarini and E. Koch (eds.): *Orbital physics in correlated matter*,
Reihe Modeling and Simulation, Vol. 13 (Forschungszentrum Jülich, 2023)
`http://www.cond-mat.de/events/correl23`

[31] E. Pavarini, E. Koch, and A.I. Lichtenstein, Phys. Rev. Lett. **101**, 266405 (2008)

[32] E. Pavarini and E. Koch, Phys. Rev. Lett. **104**, 086402 (2010)

[33] X-J. Zhang, E. Koch and E. Pavarini, Phys. Rev. B **105**, 115104 (2022)

[34] X-J. Zhang, E. Koch and E. Pavarini, Phys. Rev. B **106**, 115110 (2022)

[35] X-J. Zhang, E. Koch and E. Pavarini, Phys. Rev. Lett. **135**, 026508 (2025)